Scramjets

Michael Smart
Centre for Hypersonics
The University of Queensland
Brisbane 4072
Australia

NOMENCLATURE

A	area (m^2)		T	temperature (K)
C_f	skin friction coefficient		T_t	total temperature (K)
C_D	drag coefficient		V	velocity (m/s)
C_L	lift coefficient		w_{cap}	capture width of scramjet (m)
c_p	specific heat (J/kgK)		x	axial distance (m)
D	drag (N), hydraulic diameter (m)		α	angle-of-attack (degrees)
f	specific uninstalled thrust (m/s)		ϕ	equivalence ratio
f_{st}	stoichiometric ratio		ϑ	constant in mixing curve
F	stream thrust (N)		γ	ratio of specific heats
F_{add}	addative drag (N)		η	efficiency
F_{un}	uninstalled thrust (N)		ζ	flight path angle (degrees)
g	gravitational acceleration (m/s^2)		ρ	density (kg/m^3)
h	altitude (km), enthalpy (J/kg)			
h_{pr}	heat of combustion (J/kg of fuel)			

H_t total enthalpy (0K basis) (J/kg)

Subscript

Isp   specific impulse (s)

L	lift (N)
m	mass (kg)
m_c	mass capture ratio
$\dot{m}$	mass flow rate (kg/s)
M	Mach number
p	pressure (Pa)
q	dynamic pressure (Pa)
Q	heat (J)
R	gas constant (J/kgK)

c	combustor entrance
out	outflow
f	fuel
i	initial
in	inflow
m	mixing
n,N	nozzle
o	initial
p	payload
s	structural

1. INTRODUCTION

The desire for hypersonic flight within the atmosphere has motivated multiple generations of aerodynamicists, scientists and engineers. In the late 1950's and early 1960's it became clear that while rocket propulsion had the potential for access-to-space and the ability to reach many parts of the globe on ballistic trajectories, only an airbreathing propulsion system could facilitate practical hypersonic flight. Antonio Ferri aptly described the important differences between rockets and airbreathing engines (Ferri 1964) as:

1. The potential specific impulse of airbreathing propulsion is much larger than any chemical rocket, due to the fact it carries only fuel and not oxidiser.

2. Structural weight of an airbreathing engine is larger for the same thrust than a rocket, because it must process air (oxygen and nitrogen) and have an intake, whereas the rocket has an oxidiser tank and pressurization system.

3. The thrust of an airbreathing engine is a function of flight Mach number and altitude. Large thrust per unit frontal area can only be obtained in the dense atmosphere, while rockets can operate at high thrust per unit frontal area in a vacuum.

4. The necessity for flight in the atmosphere introduces severe structural problems for the airbreathing engine associated with aerodynamic heating and vehicle drag. However, the vehicle has a greater potential for manoeuvring than a rocket traveling in a vacuum, through the use of aerodynamic lift.

It was recognised at the time that a hypersonic airbreathing propulsion system could fulfill many roles that a rocket could not, including hypersonic cruise and recoverable space launchers. Figure 1 shows a futuristic hypersonic airbreathing vehicle concept from that time period.
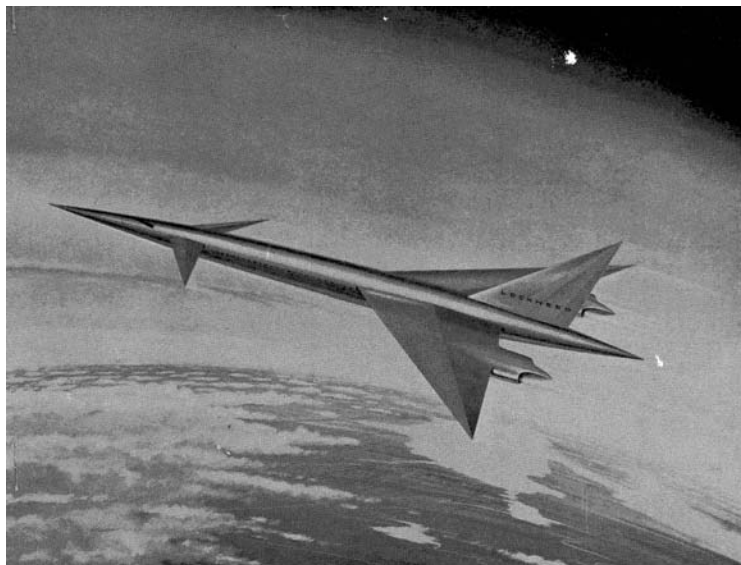

Figure 1 - 1960's hypersonic airplane

The airbreathing engine cycle best suited to hypersonic flight is the supersonic combustion ramjet, or the scramjet. This type of engine can be properly viewed as an extension of the very successful ramjet engine cycle, which uses shock wave compression in the inlet in lieu of the compressor in a gas-turbine engine. In a ramjet, air entering the combustor is first decelerated to subsonic speeds, where fuel is injected and burnt, and finally expanded through a second throat to a thrust nozzle. As flight speeds increase above Mach 5, reducing the air to subsonic conditions produces two problems; (1) significantly increased shock losses in the inlet, particularly at the terminal normal shock, and (2) significantly increased flow temperatures in the combustor. The second of these problems not only creates material/structural issues in the combustor, but leads to chemical dissociation in the nozzle expansion and a consequent energy loss from the engine cycle.

The idea of adding heat to a supersonic stream was first investigated in the late 1940's, but only attracted serious attention in the late 1950's with the investigation by Weber and McKay (1958) at the NASA Lewis Research Centre. This work compared the estimated performance of the ramjets and scramjet engine cycles at increasing Mach number using hydrogen fuel, and calculated that the scramjet cycle was superior above Mach 7. Results of a further study of the efficiency of airbreathing engines (Anderson et.

al. 2001) are shown in Fig. 2. Once again the switch over between ramjet and scramjet cycles was calculated to occur at Mach 6-7, however it was also pointed out in the same reference that the high combustor static pressure of a ramjet operating above Mach 5 may be a more important reason for choosing a scramjet cycle than fuel efficiency. As is also shown in Fig.2, as speeds increase the specific impulse of scramjets reduces, and was calculated to reach the performance level of a rocket somewhere above Mach 16.
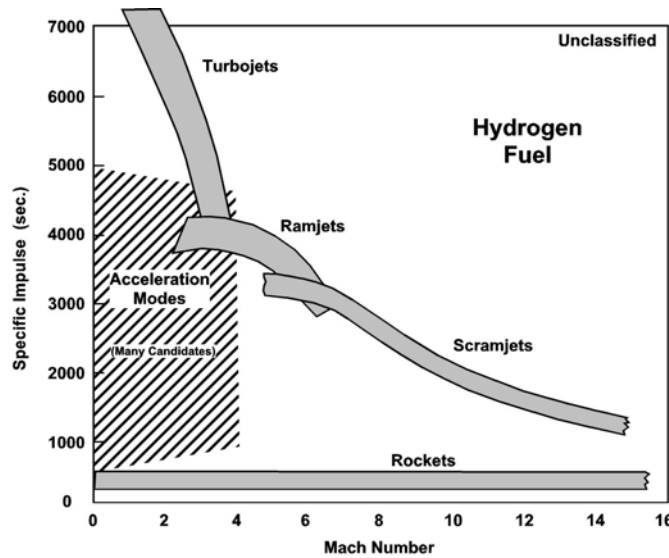

Figure 2 - Specific impusle levels for different propulsion systems

Early researchers quickly grasped the difficulties of designing scramjet engines, including:

1. Mixing and ignition of fuel and air in the short residence times of a supersonic combustor.
2. The high heat loads and friction losses that occur at hypersonic speeds.
3. The control of thermal choking.
4. Non-equilibrium nozzle flows and the loss of energy from the cycle due to incomplete combustion.

Current day scramjet designers grapple with these same issues, although we now have 40 years of experience to guide us. Two further critical issues for practical hypersonic propulsion using scramjets are:

5. No thrust production below a flight Mach number ranging from 3.5-5, depending on the particular engine design. A booster or low-speed propulsion system is therefore required to raise the vehicle to the scramjet take-over Mach number.
6. Operating over a large Mach number range with a "realistic" engine structure requires some finesse and many compromises for adequate performance at the upper and lower limits of the desired speed range.

The reason for (5) is straight forward; an engine that relies on shock compression in the inlet requires supersonic inflow, and further, if supersonic flow needs to be maintained in the combustor, this raises the lower limit for thrust production even higher.

The reasons for (6) becomes abundantly clear as soon as scramjet performance calculations are attempted at different flight Mach numbers. At lower speeds where the stoichiometric heat of combustion is relatively large compared to the kinetic energy of the airflow, combustion fuel can produce large pressure

rises in constant area combustors and possible choking or disruption to the flow through the engine, know as an unstart. Divergent combustors and/or step increases in combustor area are needed to burn a respectable proportion of the air captured by the engine in this instance. At higher speeds, however, where the kinetic energy of the airflow is significantly higher, combustor divergence can lead to chemical kinetics issues and incomplete combustion. Inlet contraction ratio requirements also change significantly with Mach number. Creating an engine that can operate over a large Mach number range is one of the key technological challenges in current times.

In this article an historical perspective on important scramjet development programmes in the United States is first presented, followed by a description of recent scramjet flight programmes. The stream thrust based cycle analysis methods used to calculate scramjet performance are then presented, followed by a description of the component analysis used to determine the performance of a scramjet. The article closes with a discussion of scramjet application to a system for acceleration to low earth orbit.

2.0 HISTORICAL PERSPECTIVE ON PAST SCRAMJET DEVELOPMENT PROGRAMMES IN THE UNITED STATES

The history of scramjet programmes throughout the world, up to the year 2000, is well described in an article by Curran (2001). Following is a short history of some past scramjet development programmes in the United States.

2.1 Scramjet Development in the United States

The 1960's saw an increased interest in scramjet propulsion, which in the United States was concentrated in two groups; one at NASA Langley Research Center, and the other supported by the US Navy at the Applied Physics Laboratory, Johns Hopkins University (APL). A significant amount of scramjet research was also conducted in industry through support from the US Air Force. These groups followed quite different technological paths leading up to the mid-1980's, when the National Aerospace Plane (NASP) Program brought most of the US scramjet community together.

Considerable experimental research on inlets and combustor components had been conducted at NASA Langley prior to 1964. This work demonstrated the validity of supersonic combustion, and indicated the potential of an integrated scramjet with hydrogen as both fuel and coolant. The Hypersonic Research Engine (HRE) Project was formulated to put this into practice, with the objectives of (a) demonstrating high internal thrust performance for a scramjet engine over a Mach number range of 4-8, and (b) development of hydrogen cooled engine structures technology (Andrews & Mackley 1994). Figure 3 shows a photograph of the HRE, which was and axisymmetric pod type configuration with a translating spike and an annular combustor. This program continued till 1974 with both a boiler plate, water-cooled model used for scramjet testing, and a flight weight, hydrogen-cooled model for structural testing.
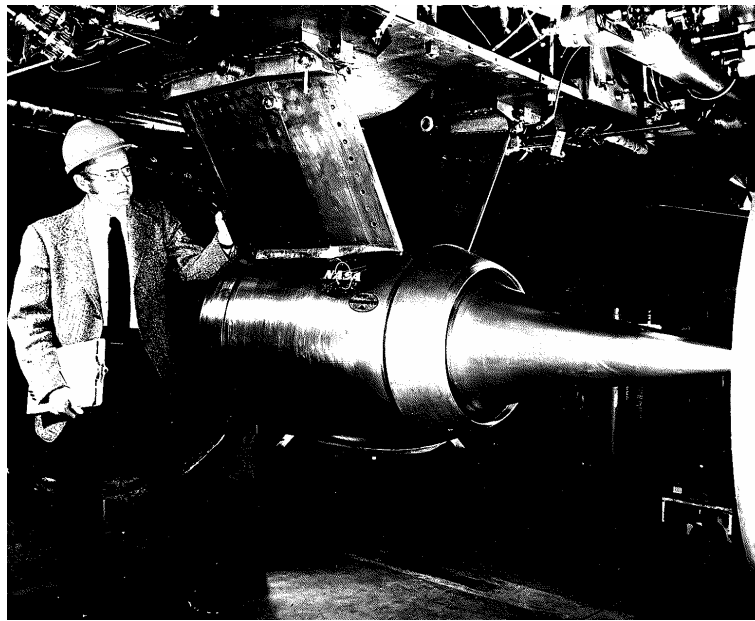
Figure 3 - HRE engine model in wind tunnel

A total of 52 scramjet tests were completed with the water cooled engine at equivalent flight Mach numbers of 5, 6 and 7 with a range staged injector options (Andrews & Mackley 1994). Figure 4 shows a plot of the calculated combustion efficiency based on the pressure measurements in the combustor at Mach 6, together with a schematic showing the different fuel injection options. A tremendous amount of knowledge about fuel ignition and combustion was gained from this testing, including a demonstration of a smooth transition from a supersonic to a subsonic combustion mode of operation. Figure 5 shows a plot internal thrust coefficient vs Mach number for the HRE at $\phi = 1$, which met the performance goals of the project. Unfortunately, the pod type configuration of the HRE also had significant external drag, and during the program it was realized that scramjet engines must be integrated with the vehicle in order to have good installed thrust.
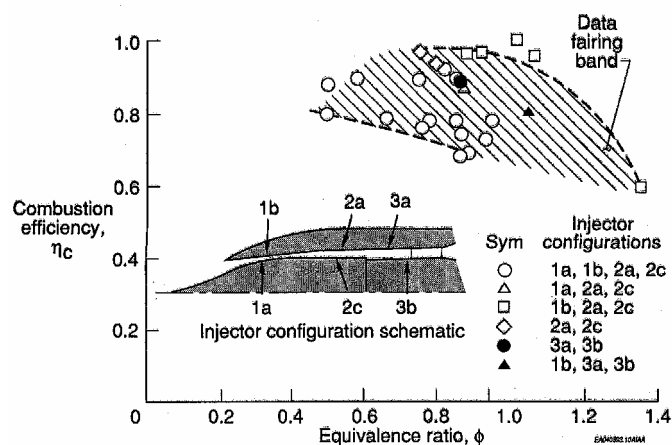

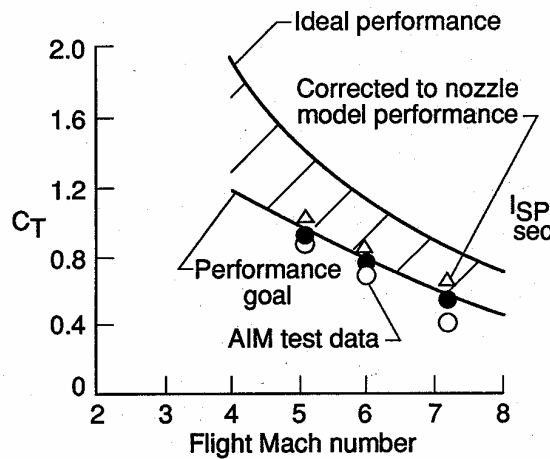**Figure 4 - HRE combustion efficiency data at Mach 6**

Figure 5 - HRE internal thrust performance

NASA Langley responded to the need for airframe integration with the 3-D swept side-wall compression scramjet. This fixed geometry configuration, a schematic of which is shown in Fig. 6, had low external drag, a rectangular cross-section, was modular in design, and fit snuggly inside the bow shock of a vehicle flying at hypersonic speed (Trexler & Souders 1975). Being a fixed geometry scramjet, these engines were designed to operate over a large Mach number range with self-starting inlets. Particular areas of research related to the development of these engines were, (1) control of the swept shock interactions in the inlet, (2) reduction of flow distortion at the inlet throat, (3) introduction of fuel injection struts to reduce engine length and weight, and (4) integration with the vehicle fore and aft bodies. Many hundreds of component and integrated scramjet tests were conducted in support of this engine concept at Langley's hypersonic facilities through the 1970's and 80's.
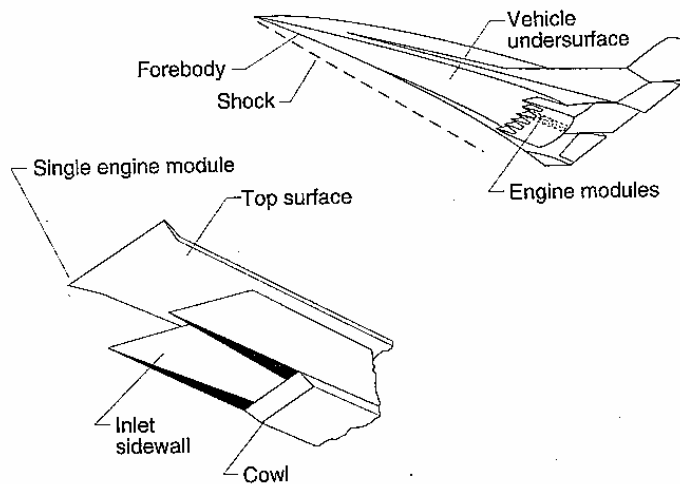

Figure 6 - Langley swept side-wall compression scramjet

Scramjet research at APL was concentrated on the hypersonic missile application rather than a large scale vehicle, hence it followed quite a different path to NASA. In the early 1960's the US Navy was interested in a Mach 6-8 follow-on to its ramjet powered missiles. The APL research was therefore concentrated on liquid hydrocarbon fuelled engines. Research was conducted to better understand the physical and

chemical processes governing supersonic combustion, and a technology database on inlets, fuel injectors, combustors, nozzles and fully integrated engines was developed during the 1960's and 70's (Waltrup 1990). Figure 7 shows one integrated scramjet missile concept to be developed at APL during this period, known as the Supersonic Combustion Ramjet Missile (SCRAM), which was designed for maximum cruise at Mach 8 (Billig 1995). In 1978, emphasis was placed on development of the Dual Combustor Ramjet (DCR), which used conventional liquid hydrocarbon fuels and had a maximum Mach number of 6. A schematic of the engine concept is shown in Fig. 8, showing a missile with a spike nose, both supersonic and subsonic inlets, fuel injection into the flow processed by the subsonic inlet, and a supersonic combustor leading to a thrust nozzle (Waltrup 1990). Development of this concept continues today as part of the DARPA HyFly Program.
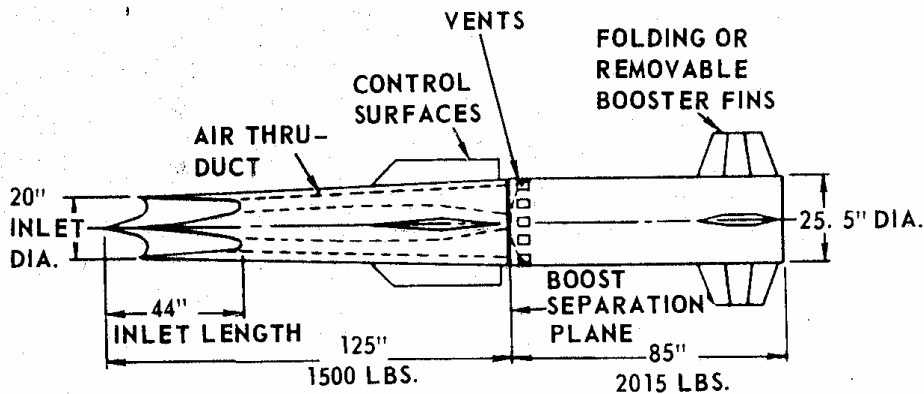

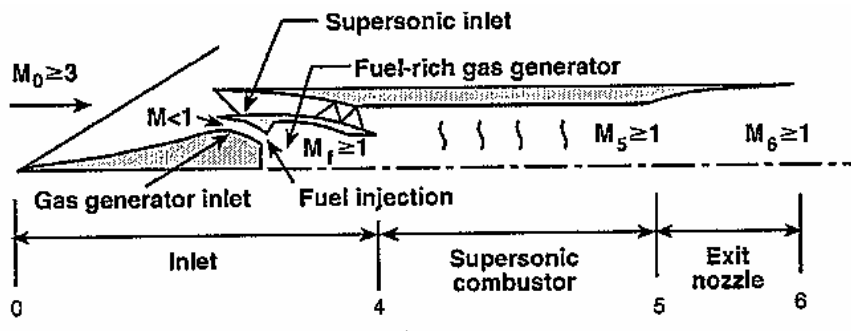Figure 7 - APL Supersonic Combustion Ramjet Missile

Figure 8 - Schematic of the APL DCR engine concept

A significant amount of scramjet configuration development and testing was supported by the US Air Force during the 1960's. This involved numerous industry contractors, including General Electric, Marquardt, United Technologies Research Laboratories, and General Applied Science Laboratories (GASL). One product of this support, shown in Fig. 9, was developed by GASL and called the low-speed fixed geometry scramjet. It was designed to operate from Mach 3-12 with fixed geometry, and used fuel scheduling and thermal compression effects in place of variable geometry. It was tested at Mach 7.4 at the GASL hypersonic facilities in 1968.
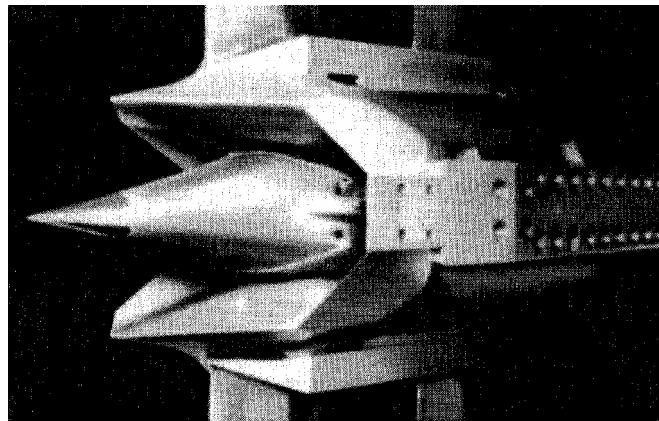
Figure 9 - GASL Mach 3-12 scramjet

The one project that combined most (if not all) US knowledge of hypersonic airbreathing propulsion, was the National Aerospace Plane (NASP) Program. This aggressive effort was initiated in 1985 by the Defense Advanced Research Projects Agency (DARPA) with the goal of developing a single-stage-to-orbit (SSTO) airplane called the X-30 (Barthelemy 1989). This vehicle was envisioned to take-off horizontally under gas-turbine power, accelerate to low earth orbit insertion velocity (Mach 25) through the use of hydrogen-fuelled scramjets and rockets, and then return to earth for horizontal landing. It really was a "space-plane" which would have brought aircraft-like operational flexibility to space. The seminal study at the beginning of the project was by Tony Du Pont, a schematic of which is shown in Fig.10. The Du Pont vehicle weighed 50,000 lb at take-off, used hydrogen fuel and a combined cycle air-breathing engine.
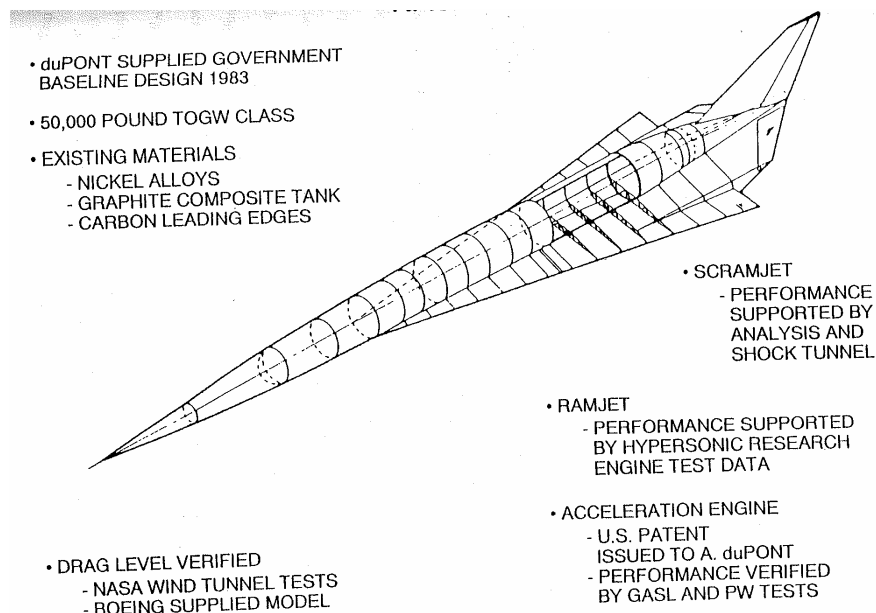

Figure 10 - Original space plane concept for NASP

Over its 10-year span the NASP Program involved NASA, the US Air Force, APL and a large contingent of industry players (Schweikart 1998). Many scramjet configurations were designed and tested in various facilities (Andrews 2001), and the understanding of air-breathing hypersonic propulsion was considerably deepened. Some examples of hardware tested during the NASP program are shown in Figs.11 and 12.

The 3-D sidewall compression inlet model in Fig. 11 was based on a Rocketdyne (Rockwell) engine concept with heritage to earlier NASA Langley engines of similar configuration. The two-dimensional engine model in Fig.12 was known as the Concept Demonstration Engine (CDE), and was tested towards the end of the NASP program at simulated Mach 6.8 flight conditions in the 8-Foot High Temperature Tunnel at NASA Langley (Voland & Rock 1995).

Figure 11 - 3-D Sidewall compression inlet model

Figure 12 - 2-D engine model tested at Mach 6.8

An artists impression of a possible NASP configuration is shown in Fig. 13. While not producing its goal of a working X-30 aircraft, the NASP Program spurred the development of many technologies related to hypersonics, including computation fluid dynamics, high temperature materials and light-weight aerospace structures. It was also the genesis for the Hyper-X flight Program. Most current concepts for air-breathing access-to-space have moved away from SSTO systems, and make use of the significant advantages of multiple stage vehicles.

Figure 13 - Proposed NASP configuration

3.0   SCRAMJET FLIGHT PROGRAMMES

The flight corridor for hypersonic airbreathing vehicles, either for cruise or ascent to low-earth-orbit, is constrained at upper altitude by the need to operate the airbreathing engine, and at lower altitude by structural limits of the vehicle. Figure 14 gives an indication of these limits, and includes a suggested ascent trajectory for an airbreathing SSTO vehicle (Hunt & Rausch 1998) with the applicable range of different propulsion cycles indicated. The goal of all scramjet flight testing is to fly scramjets at some point, or over some range, within this flight corridor. Three scramjet flight programmes will be reviewed here; (1) a joint CIAM/NASA flight test conducted in 1998, (2) the HyShot 2 flight conducted by The University of Queensland in 2002, and (3) NASA's Hyper-X which flew twice in 2004.
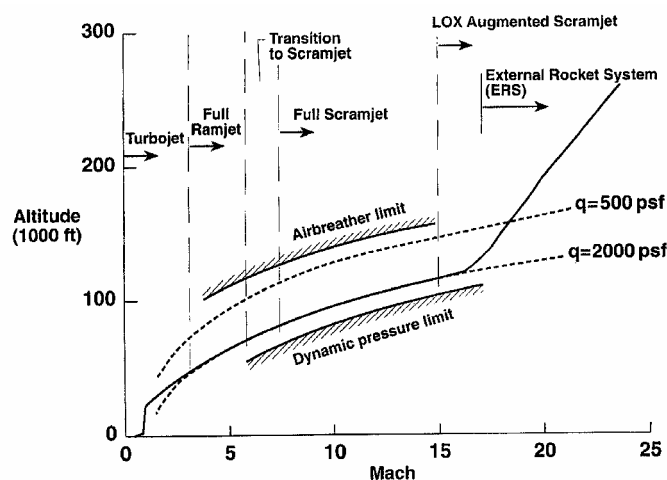

Figure 14 - Hypersonic airbreathing flight corridor

3.1   CIAM/NASA Flight Test

The Russian Central Institute of Aviation Motors (CIAM) performed a flight test of a CIAM-designed, hydrogen-cooled/fueled scramjet engine over a Mach number range of approximately 3.5 to 6.4 on February 12, 1998, at the Sary Shagan test range in Kazakhstan (Voland et. al. 1999). This rocket-boosted, captive-carry test of the axisymmetric engine reached the highest Mach number of any scramjet engine flight test at that time, and achieved 77 seconds of liquid hydrogen regeneratively cooled engine operation. The programme was conducted with NASA support and technical assistance from Langely Research Center. The engine used staged fuel injection through angled sonic holes and cavity flame holders, and was designed for dual-mode combustion. Analysis of the flight data indicated that an unexpected control sensor reading caused non-optimal fuelling of the engine, and flowpath modifications added to the engine inlet during manufacture caused markedly reduced inlet performance. Both of these factors contributed to the engine operating primarily in a subsonic combustion mode, with a peak combustion efficiency of 77.5%. Ground test data was obtained at similar conditions to flight, allowing for a meaningful comparison between the ground and flight experiments. The results of this comparison indicated that the differences in engine performance between ground and flight were small.

3.2   HyShot 2

The Centre for Hypersonics at the University of Queensland had routinely performed scramjet testing in shock tunnels since the early 1980's (Stalker et. al. 2006). Based on the desire to validate such testing for conditions in the Mach 7-8 regime, a sounding rocket based flight project known as HyShot was devised around 1997. This project involved two flight tests of a simplified supersonic combustion experiment designed solely through shock tunnel testing. While the HyShot scramjet payload was elegantly simple and quite robust, significant issues associated with providing suitable scramjet flight test conditions with the available rocket needed to be overcome. The chosen solution to these issues resulted in a highly parabolic trajectory, with the scramjet experiment being conducted during an almost vertical re-entry (Paull et. al. 2002). Following a first launch failure on October 30th 2001, the University of Queensland conducted a successful second launch on July 30th, 2002.

Both HyShot flights took place at the Woomera Prohibited Area Test Range in central Australia. Each used a two-stage Terrier-Orion Mk70 rocket that generated a highly parabolic trajectory to boost the payload and the exhausted second stage Orion motor to an apogee in excess of 300km, as shown in Fig. 15. This combination of rocket and trajectory allowed the payload and attached second stage to re-enter the atmosphere with a Mach number in excess of 7.5 between 35 and 25 km altitude, thus supplying a range of conditions within the flight corridor of Fig. 14.
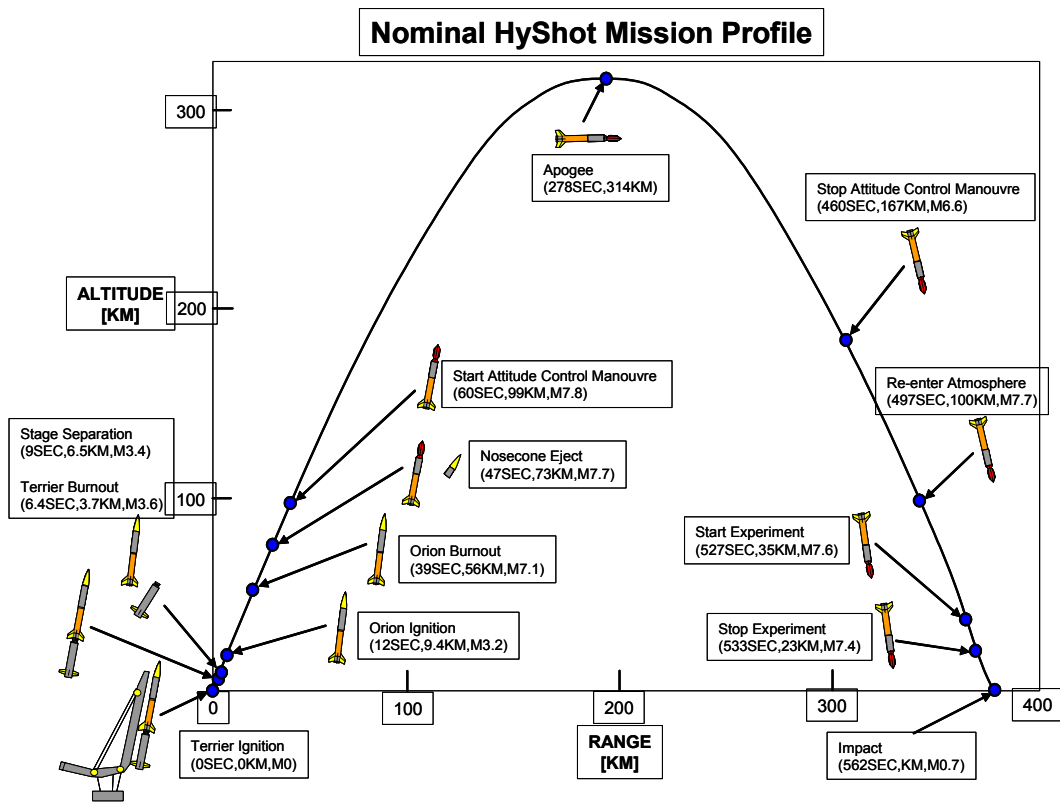
Figure 15 - HyShot flight profile

The HyShot payload included a nose-cone to shroud the scramjet flowpaths on the initial ascent, two scramjet combustors orientated back-to-back on a wedge forebody, plus hydrogen and nitrogen tanks, batteries, telemetry system, flight computer and other components. One combustor was hydrogen fuelled through 4 laterally spaced normal injectors, while the other combustor was unfuelled so as to obtain baseline (tare) conditions to compare against the fuelled flowpath throughout the flight. Figure 16 shows a photograph of the payload used for HyShot 2 (with the shroud removed). It was constructed predominantly of copper alloy for rapid dissipation of aerodynamic and combustion generated heat loads, with TZM (tungsten-zirconium-molybdinum) used for the highest heat flux regions that occur at the leading edges of both combustors.

Figure 16 - HyShot payload

The goal of the experiment was to supply uniform flow into the two rectangular combustors at conditions ranging between Mach 7.2 and 8.0, allowing for an angle-of-attack (α) variation of the payload between +5 and -5 degrees. Figure 17 shows a schematic of the fuelled flowpath. The intake consisted of a single 18 deg. wedge with a width of 100mm, a blunted leading edge, and highly swept side fences. The high wedge angle was necessary to ensure that the combustor entrance temperature and pressure were great enough to readily induce self-ignition of hydrogen. The rectangular combustor had a constant area 9.8 mm x 75 mm cross-section and a length of 300 mm (length/height = 30.61). The combustor cowl spanned the full width of the intake wedge and was situated such that the intake shock was upstream of its leading edge at all times. The flowpath design incorporated a shock trap that was situated between the end of the intake wedge and the entrance of the combustor. This feature not only captured the cowl shock, but also bled off the intake boundary layer. The reduced width of the combustor (relative to the intake wedge) and lateral spillage holes in the side fences adjacent to the shock trap were designed to remove the fence boundary layers and corner flows. The angle-of-attack of the payload was defined as positive when the fuelled combustor was on the windward side, and negative when the fuelled combustor was leeward.
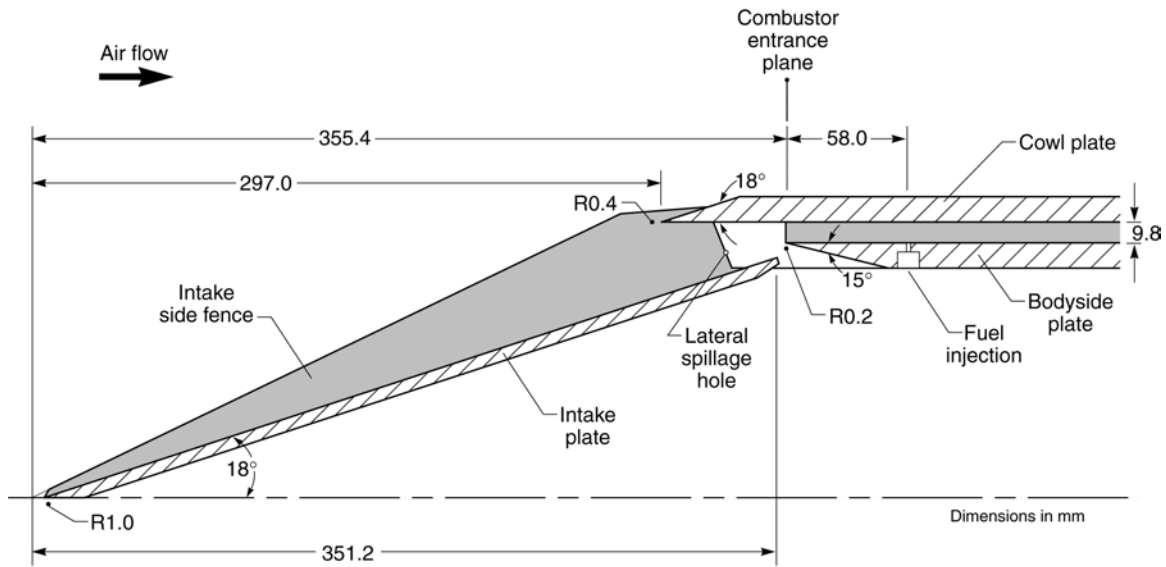
Figure 17 - Schematic of fuelled flowpath

The flight produced a significant set of scramjet combustor data at varying duct entrance pressure, temperature and Mach number. Trajectory reconstruction was accomplished using onboard sensors alone (Cain et. al. 2004). Fuel flow was initiated at approximately t = 536.5 seconds after launch as the payload and attached Orion motor re-entered the atmosphere. Figure 18 shows the Mach number and dynamic pressure time histories during three seconds of the experimental window, and Table 1 lists four zero-yaw time slices used for analysis. Figure 19 shows a comparison of the fuelled and unfuelled combustion pressure distributions at windward conditions: i.e. when each duct was at a positive angle-of-attack of approximately 5 degrees. Note that all data is normalized by the combustor entrance pressure, in order to make meaningful comparisons. The equivalence ratio of the fuelled duct was approximately 0.34, and the pressure rise from combustion of the hydrogen fuel is clearly evident. Cycle analysis of this data indicated that supersonic combustion occurred at these times slices during the flight, at a combustion efficiency for the fuel of 81% (Smart et. al. 2006).
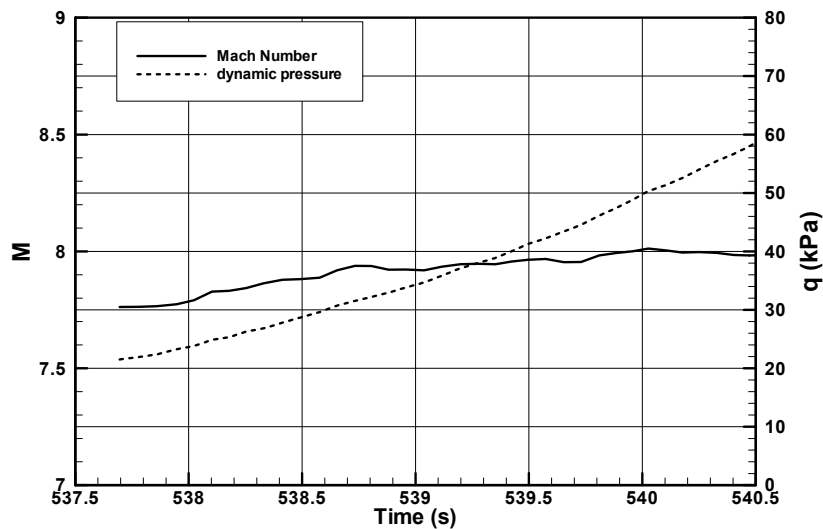

Figure 18 - Reconstructed Mach number (M) and dynamic pressure (q) histories

Table 1 – Flight parameters for analysed time slices

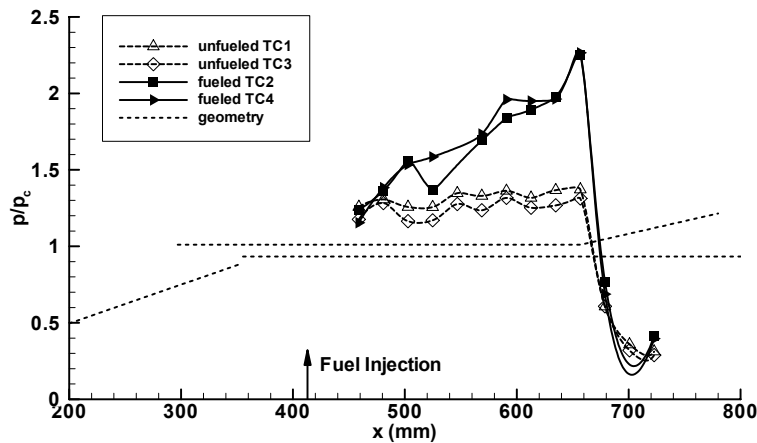| number	Time (s)	Flight Mach Number	Flight dynamic pressure (kPa)	Altitude (km)	angle-of-attack(deg.)
1	538.103	7.828	24.88	34.48	-5.012
2	538.179	7.831	25.33	34.31	5.540
3	538.734	7.938	31.55	33.05	-5.081
4	538.805	7.938	32.20	32.89	4.617

Figure 19 - Windward fueled and un-fueled combustor pressure distributions
(x = axial distance from nose of payload)

The success of the HyShot 2 flight led to a significant interest in low cost scramjet flight-testing using sounding rocket boosters. Two further flights, HyShot 3 and 4 were conducted by The University of Queensland in March 2006; HyShot 3 for the British Company, Qinetiq, and HyShot 4, for the Japanese Aerospace Agency (JAXA). Further flights are planned.

3.3   Hyper-X

NASA's focused hypersonic technology program, called Hyper-X, conducted the most realistic flight tests of hypersonic airbreathing engines to date. Unlike either the CIAM flight test or HyShot 2, the Hyper-X flight vehicle separated from its booster to fly a controlled hypersonic trajectory under scramjet power. Two successful flights were conducted; the first at Mach 7 on March 27, 2004, and a second at Mach 10 on November 16, 2004. Both included 5+ seconds of hydrogen fuelled scramjet operation, followed by a series of hypersonic aerodynamic manoeuvres as the vehicle decelerated. The key results of the flights were that:

1. Airframe integrated scramjet powered vehicles can fly stable, controlled trajectories at hypersonic speeds.

2. Accelerating hypersonic flight is possible at Mach 7 using air-breathing propulsion.

3. Hypersonic cruise is possible at Mach 10 with a non-optimised vehicle/engine combination.

4. Ground test experiments, CFD analysis and other aerodynamic tools can be used to design scramjet powered flight vehicles.

The Hyper-X vehicle, a schematic of which is shown in Fig. 20, had significant heritage from the NASP program. It was a "smart scaled" version of a 200 ft operational vehicle (Rausch et. al. 1997) that could be

flight tested within available budgets, while also demonstrating operation of a dual-mode hydrogen fuelled scramjet. The chosen 12 ft vehicle had a single airframe-integrated scramjet and was boosted to flight conditions using a modified Pegasus booster that was air-launched from a B-52 from Edwards AFB in California. The desired test conditions were 95,000 ft (~29.0 km) at Mach 7, and 110,000 ft (~33.5 km) at Mach 10, both of which correspond to a dynamic pressure of 1000 psf (~ 48 kPa). The flight sequence for the Mach 7 flight is shown in Fig. 21 (Voland et. al. 1998). The free-flying portion of the flight included separation from the booster, engine cowl opening, 5+ seconds of scramjet operation, fuel-off flight with the cowl open, and aerodynamic manoeuvres with the cowl closed. A similar sequence was conducted at Mach 10. The vehicles flown on the two flights were nominally of the same external shape, but had different thermal protection systems and different engine designs.
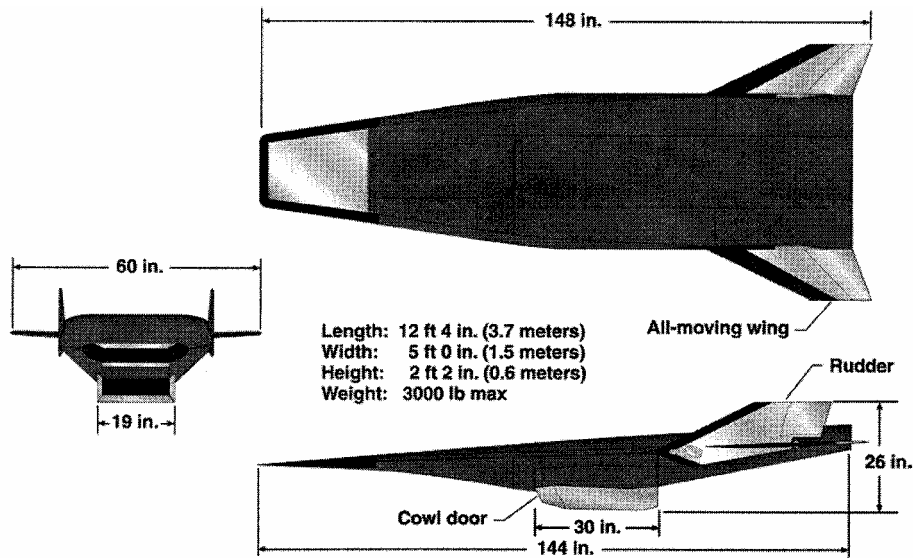

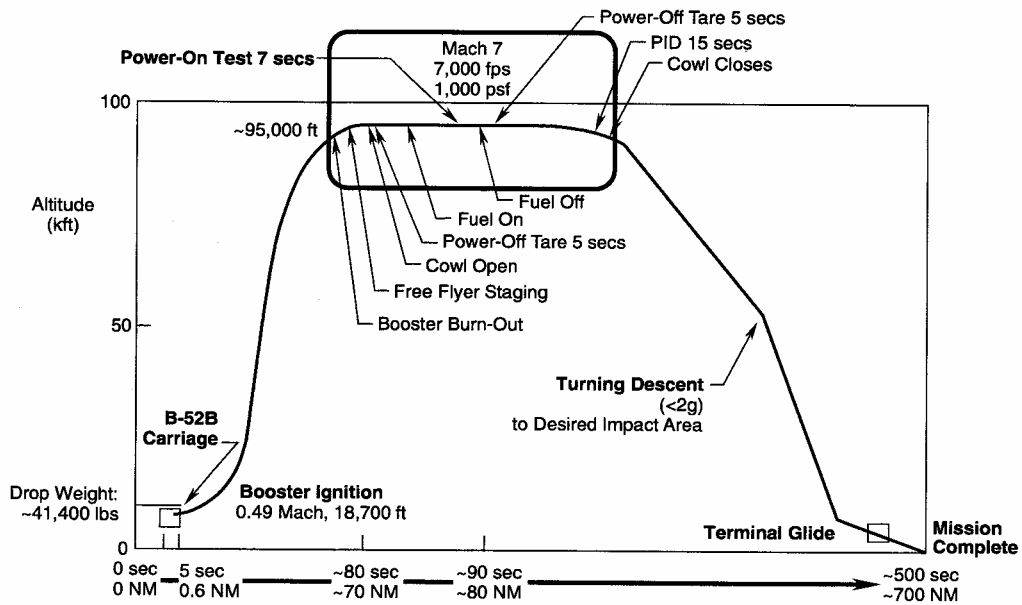**Figure 20 - Hyper-X vehicle configuration**

Figure 21 - Nominal Mach 7 Hyper-X flight trajectory

In terms of the scramjet flowpath, the Hyper-X vehicle enabled testing of a complete forebody, internal engine, and aftbody/thrust nozzle. The Mach 7 engine was developed through a long series of partial flowpath and subscale testing at NASA Langley Research Center, followed by a complete tip-to-tail flowpath simulation in the 8 foot High Temperature Tunnel (8-FT HTT), also at NASA Langley. A photograph of the engine, known as the Hyper-X Flight Engine (HXFE), is shown in Fig. 22. It was mounted upside down in the test section of the 8-FT HTT on a force balance with identical internal system components to those used in flight. The main objectives of this pre-flight testing were to validate the Mach 7 propulsion database and to verify the operation of system components. Not only were the engine operability and performance data acquired during testing, but realistic estimates of the aero-propulsive vehicle force and moment increments due to both opening the cowl door and combustion were obtained (Huebner et. al. 2001).
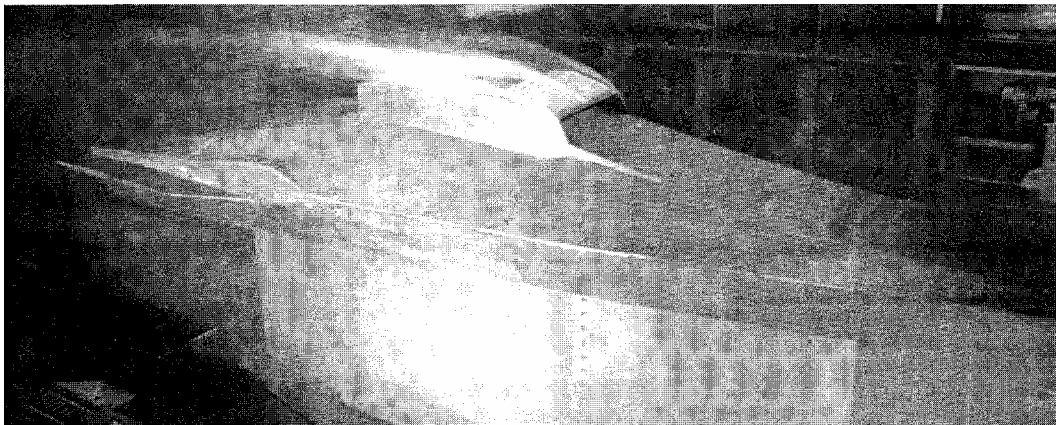

Figure 22 - HXFE engine in 8-FT HTT (flow from right to left)

Figure 23 shows a comparison of the body and cowlside pressure distributions in the Hyper-X engine between 8ft-HTT ground tests and flight, at the design throttle level (Ferlemann et. al. 2005). These results indicate very little difference between ground and flight data, which were closely matched in terms dynamic pressure and Mach number. The main difference between the two experiments was the flow contaminants in the 8ft-HTT (H_2O and CO_2), which appear to have little effect on the engine performance at these conditions and throttle level.
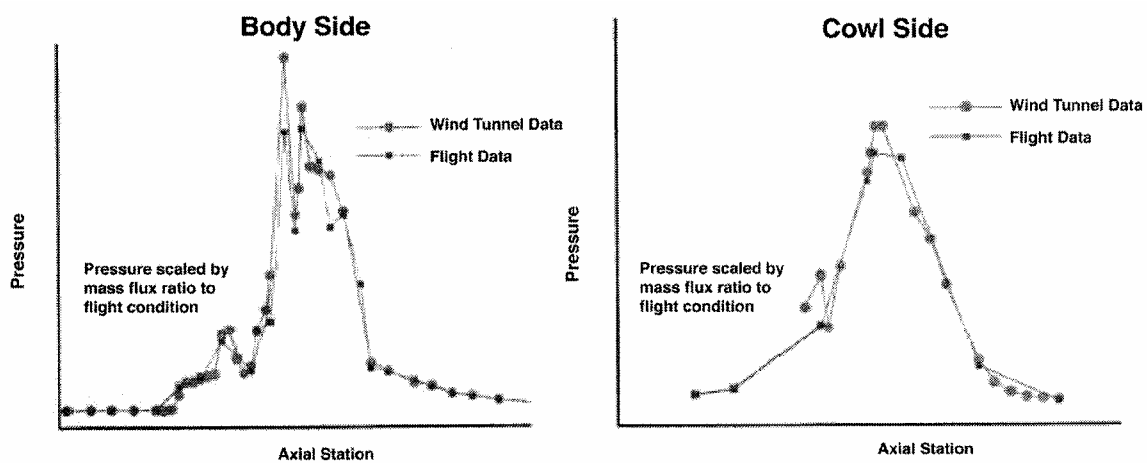

**Figure 23 - Comparison of ground and flight data for the
Hyper-X Mach 7 flight at design throttle level**

While the Mach 7 engine was able to be ground tested in long duration facilities, only impulse facilities can generate conditions to simulate Mach 10 propulsive flight on the ground. The ground tests to support development of the Mach 10 engine were done at the NASA HyPulse Shock tunnel situated at GASL's New York facility. This meant that only instantaneous testing was possible, and engine sequences such as piloting and fuel ramp-up could not be simulated. Despite this, the Mach 10 engine performed to expectation, as indicated in Fig. 24, which shows a comparison of prediction and flight pressure distributions on the bodyside of the Mach 10 engine taken from McClinton (2006).
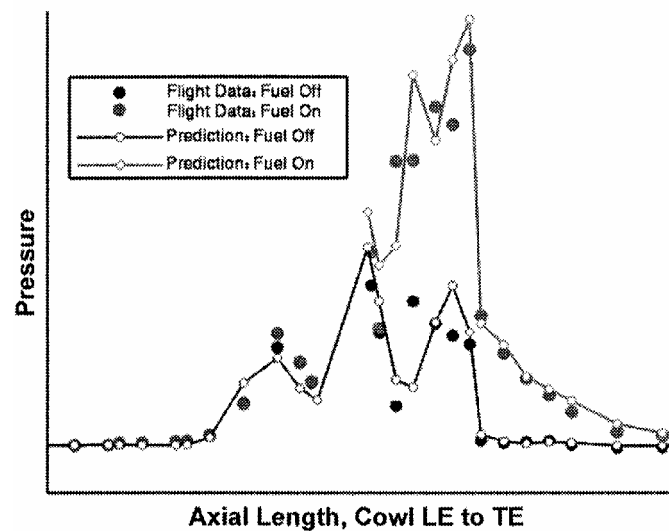

Figure 24 - Comparison of prediction to flight for the Hyper-X Mach 10 flight at design throttle position

Since Hyper-X, the United States Air Force has initiated the X-51 program, which is planned to include multiple flights of a liquid hydrocarbon missile-like configuration. The DARPA has funded the HyFly Program, which is based on the APL DCR configuration. Finally, a ten flight sounding rocket based programme called HiFIRE was recently initiated by the Defence Science and Technology Organisation (DSTO) of Australia and the United States Air Force. The goal of this programme is to develop the technology required for long duration scramjet flight at Mach 8.

4.0 SCRAMJET PERFORMANCE ANALYSIS

The performance of a scramjet engine, either uninstalled or when integrated on a hypersonic vehicle, is most easily determined by what is called stream thrust analysis. This technique conserves the fluxes of mass, momentum and energy on strategically placed control volumes to determine the propulsive forces on the vehicle. Figure 25 shows a schematic of a scramjet powered vehicle with a control volume surrounding all the airflow that passes through the engine. Airflow enters the control volume at the flight conditions, fuel is added to the air in the combustor and the flow exits through the vehicle nozzle. For ease of analysis, the flow exiting the control volume is usually represented by a flux-conserved one-dimensional average of the non-uniform exhaust plume. In the current analysis only the axial forces will be considered, however, similar relations can be developed for the transverse direction to determine the lift forces generated by the propulsion system.
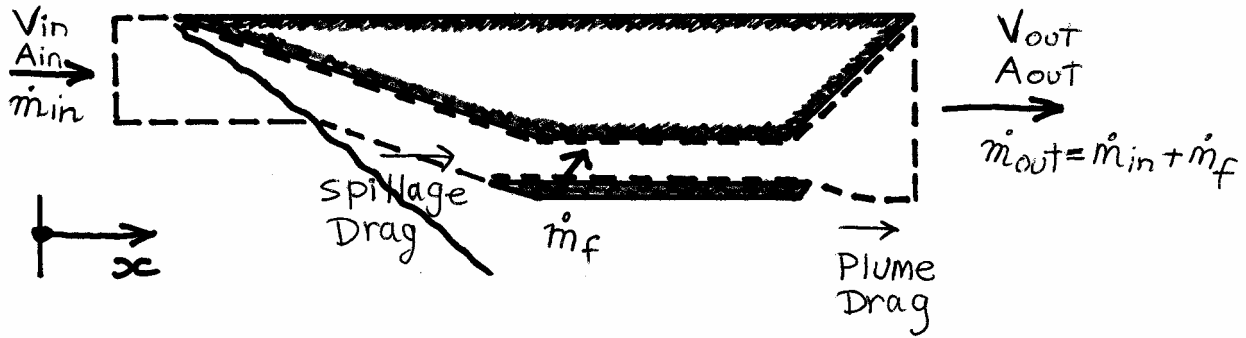
Figure 25 - Schematic of control volume used for scramjet performance analysis

Assuming for simplicity that fuel is added with no component of velocity in the streamwise direction, application of Newtons law to the control volume in Fig. 25 in the streamwise direction yields the following relation:

$$\dot{m}_{in} V_{in} + p_{in} A_{in} - (\dot{m}_f + \dot{m}_{in}) V_{out} + p_{out} A_{out} + \sum F_{xs} = 0 \qquad (1)$$

where $\sum F_{xs}$ = sum of the pressure and viscous forces on the top and bottom boundaries of the control volume.

It is customary to separate the addative drag due to inlet spillage and the nozzle plume from $\sum F_{xs}$ as follows:

$$\sum F_{xs} = F_{add} + F_{surface}$$

Re-arranging eqn. 1 yields:

$$F_{surface} = (\dot{m}_f + \dot{m}_{in}) V_{out} + p_{out} A_{out} - \dot{m}_{in} V_{in} - p_{in} A_{in} - F_{add} \qquad (2)$$

The left hand side of eqn. 2 is the thrust of the uninstalled engine, F_{un}. Using the definition of stream thrust, $F = pA + \dot{m}V$, we can express eqn. 2 as:

$$F_{un} = F_{out} - F_{in} - F_{add} \qquad (3)$$

Equation 3 indicates that the uninstalled thrust of an engine can be determined with knowledge of the stream thrust of the air entering the engine, the addative drag, and the stream thrust exiting the engine nozzle. The flow enters the engine at ambient conditions and at the flight velocity, so determination of F_{in} reduces to a determination of the freestream capture area. Air spillage (and therefore spillage drag) decreases as the vehicle speed approaches the design point, and the plume drag varies depending on the amount of under-expansion in the nozzle. Both these are usually estimated through CFD analysis, or through rules-of-thumb based on empirical or experimental databases. Determination of F_{ex} requires an involved analysis that follows the air through the complete scramjet flowpath. Many authors have presented analyses to calculate F_{ex} for complete scramjet flowpaths with differing levels of sophistication and accuracy (Heiser & Pratt 1994, Pandolfini 1986, Pinckney et. al. 2004). The analysis presented here is in the form used by the present author.

4.1   Scramjet Component Analyses

Figure 26 shows a schematic of the internal flowpath of an airframe-integrated scramjet with particular reference stations highlighted. In keeping with the convention of Heiser & Pratt (1994), station 0 is in the freestream flow ahead of the engine, and a streamtube with area A_0 is captured and processed by the engine. Station 1 is downstream of the vehicle forebody shock and represents the properties of the flow that enters the inlet. Station 2 is at the inlet throat, which is usually the minimum area of the flowpath, and the length between stations 2 and 3 is referred to as the isolator. Station 3 represents the start of the combustor, and fuel and air is mixed and burned by the end of the combustor at station 4. The nozzle includes an internal expansion up to station 9, and an external expansion to station 10 at the end of the vehicle.
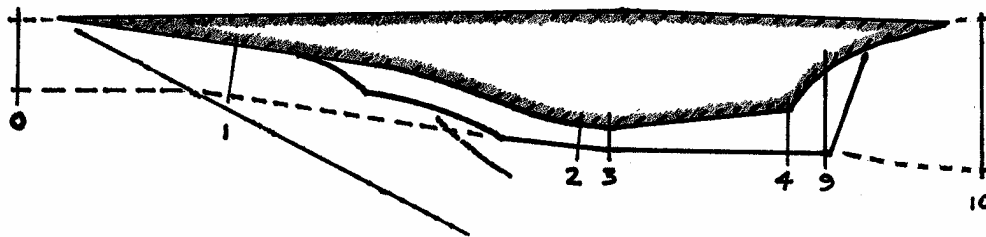

Figure 26 - Flow stations for engine analysis

It is appropriate to break the analysis needed to determine the stream thrust of the flow exiting the vehicle, and therefore the uninstalled thrust of the engine, into the three processes that make up the engine cycle; i.e. those of compression, combustion and expansion. While the compression and combustion processes can be blurred for some operating conditions, this convention will be adhered to here.

4.1.1   Compression

Efficient combustion of fuel requires that air be supplied to the combustor at a suitable pressure, temperature and mass flow rate. For a scramjet traveling at speeds greater than Mach 5 and at altitudes in the flight corridor of Fig. 14, this requires significant compression and heating of the air. For an airframe-integrated scramjet, both the vehicle forebody and inlet share this task. A multitude of different forebody/inlet configurations have been developed by many researchers (Van Wie 2001), each designed to generate a specified level of compression over a range of flight Mach numbers. The performance of such compression systems can be separated into two key parameters; (1) inlet capability, or how much compression is performed, and (2) inlet efficiency, or what level of flow losses does the inlet generate during the compression process. Meaningful discussions of inlet performance must include both parameters as, for example, a highly efficient inlet can be very easily designed if it is required to do little compression.

Performance analysis of scramjet inlets involves the determination of the flow conditions at the inlet throat (station 2 of Fig. 26). A common parameter used to quantify the efficiency of the forebody/inlet compression is the kinetic energy efficiency, η_{KE}. The usefulness of this parameter, compared to many others, is that it can be used for non-ideal gas processes, and that its value has been found to be relatively independent of Mach number for a given class of inlets. The definition of η_{KE} is simply the ratio of the kinetic energies of the flow before and after the compression, and is most easily described on a Mollier diagram, as shown in Fig. 27. Here the flow entering the engine is compressed from p_0 to p_2. During the compression there is heat loss to the forebody/inlet structure, and:

$$\eta_{KE} = \frac{1/2\,u_2^{\,2}}{1/2\,u_0^{\,2}} = \frac{h_{t2} - h_2}{h_{t0} - h_0} \qquad (4)$$
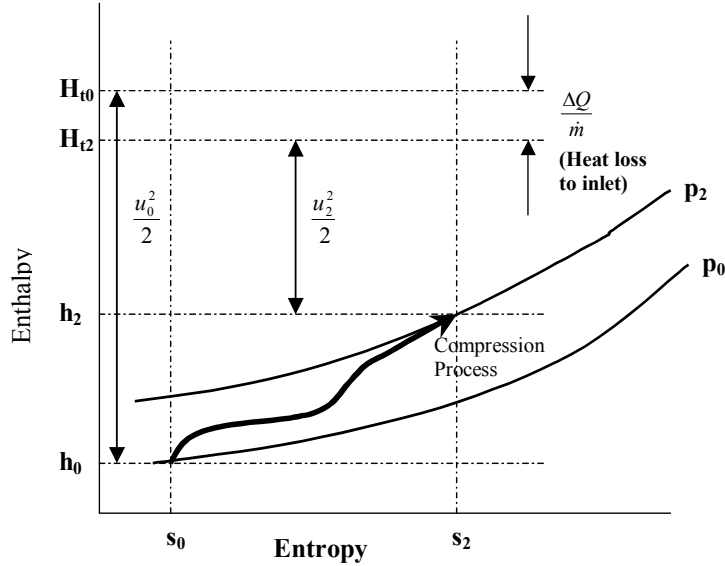

Figure 27 – Mollier diagram of inlet compression process

In some instances the adiabatic kinetic efficiency, $\eta_{KE,ad}$ is used. This parameter does not account for heat loss, and is defined as:

$$\eta_{KE,ad} = \frac{h_{t0} - h_2}{h_{t0} - h_0} \qquad (5)$$

When conducting scramjet performance calculations, two common methods for determining the properties at the inlet throat are; (1) use an empirical relation for η_{KE} in combination with a number of other parameters, and (2) use CFD to perform a numerical simulation of the forebody/inlet flowfield. An empirical correlation for $\eta_{KE,ad}$ in terms of the ratio of throat Mach number to freestream Mach number, M_2/M_0, is as follows (Waltrup et. al. 1982):

$$\eta_{KE,ad} = 1 - 0.4 \left\{ 1 - \frac{M_2}{M_0} \right\}^4 \qquad (6)$$

This expression relates inlet efficiency to an inlet capability parameter, M_2/M_0, so it satisfies our requirement for being a useful relation. However, in order to determine flow properties at the inlet throat, a temperature ratio, (T_2/T_0), an average ratio of specific heats, γ_{av}, and an amount of heat loss to the vehicle must be also be specified. Figure 28 compares this correlation with a summary of reported inlet efficiency values for a range of inlet geometries. It appears that for first order accurate performance calculations, eqn. 6 is a reasonably choice for modeling scramjet compression processes.
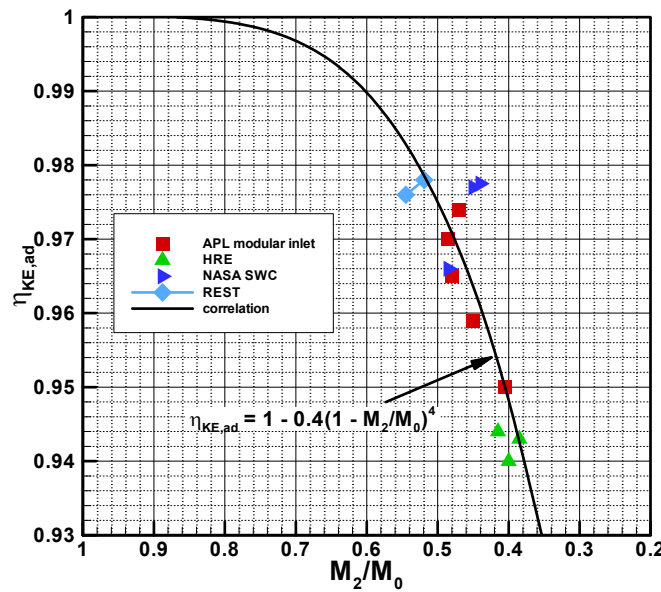
Figure 28 - Inlet efficiency data (subscript 4 corresponds to the inlet throat)

Since the mid-1990's, modern computers and CFD codes have developed to the point where the calculation of turbulent flows through hypersonic inlets can be performed on a routine basis. A more accurate model of the scramjet compression process for a particular configuration can therefore be obtained through multiple CFD calculations over the operational flight Mach number. An example of this is shown in Fig. 29, where the flux-conserved, one-dimensional averaged inlet throat properties and mass capture ratio are plotted for a 2-D forebody/3-D inlet combination based on CFD calculations over a range of inlet Mach number, M_1 (Smart & Tetlow 2006).
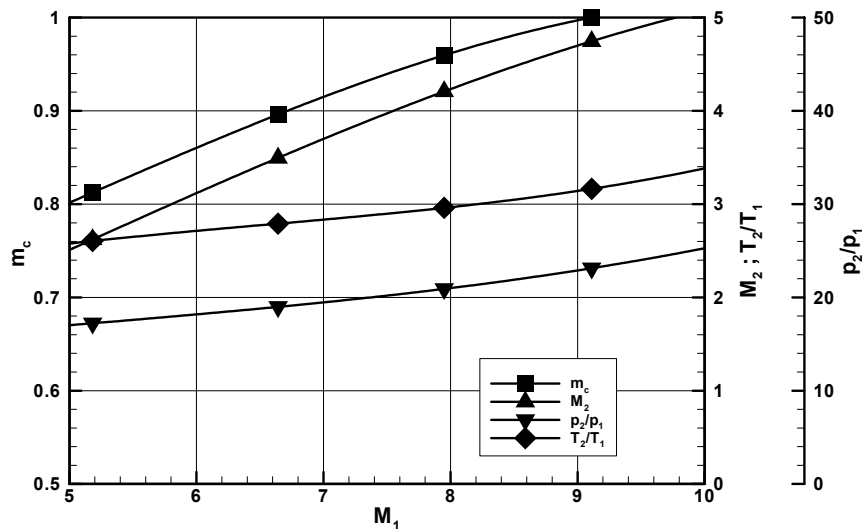

Figure 29 – CFD based Inlet capability parameters

In the design of hypersonic inlets there are some key issues that must be addressed in order to arrive at a useful configuration. These are:

1. Inlet starting limits

2. Boundary layer separation limits

3. Minimization of external drag

4. Performance at off-design Mach number

The process of establishing supersonic flow through the inlet, known as inlet starting, puts a significant constraint on the internal contraction ratio of hypersonic inlets. This can be overcome through variable geometry, however, the weight/complexity of such can significantly degrade the overall system performance of a scramjet engine. Figure 30 shows a plot of the internal contraction ratio limit for self-starting of a range of inlet configurations, as well as a theoretical starting limit developed by Kantrowitz & Donavon (1945), which is known to be conservative at hypersonic Mach numbers. In general, the self-starting limits of particular inlet classes are determined through experimental testing, and become more restrictive as the starting Mach number is decreased.
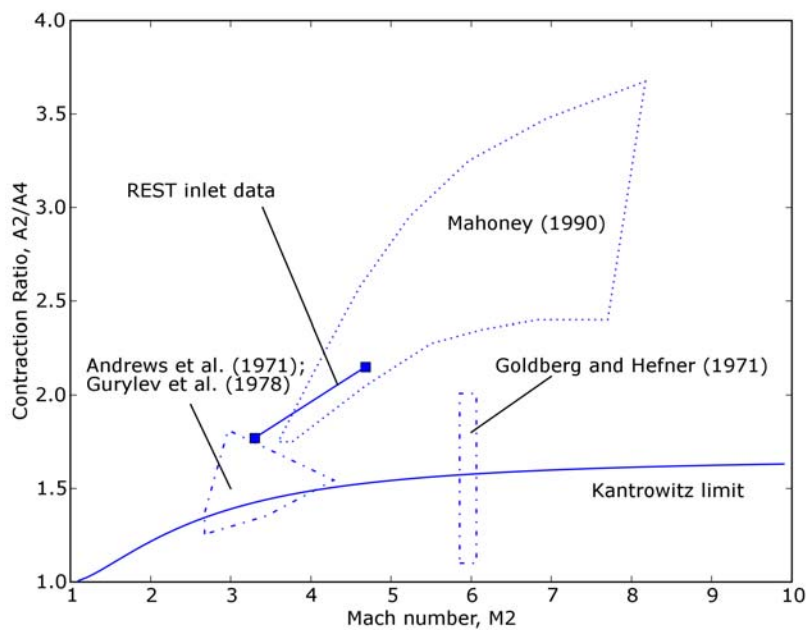

Figure 30 - Selected experimental data on starting limits with comparisons to the Kantrowitz limit (subscript 2 corresponds to the closure plane of the inlet; subscript 4 corresponds to the inlet throat)

The flow through any practical hypersonic inlet will be turbulent, and can be prone to boundary layer separation due to shock interactions. While minor boundary separation may be acceptable, large-scale boundary layer separation can create blockage of the engine and inlet unstart. Inlet flows are therefore required to satisfy established boundary layer separation limits (Korkegi 1975).

The minimization of external drag is an important aspect of the inlet design process. The external drag on the inlet will always be an important parameter when comparing the performance of different inlet configurations. Finally, most inlet design methods are based on a particular design Mach number, usually at the upper limit of the operational Mach number range. Adequate off-design performance; i.e. at Mach numbers lower than the design point, is required, otherwise the vehicle will never reach it's design point.

4.1.2   Combustion

Analysis of the combustion process in a scramjet usually involves quasi-one-dimensional cycle analysis methods. While the real combusting flow in a scramjet is far from uniform at any cross-section throughout the engine, when used properly, these techniques provide an efficient means of modeling this region of a scramjet. While some methods simply jump from the start to the end of the combusting zone (Pandolfini 1986), the method presented in this article enables prediction of the pressure distribution in the entire region of the engine affected by combustion, therefore enabling comparison with experiment. These methods follow directly from the classical quasi-one-dimensional gasdynamics presented by Shapiro (1953).

At flight speeds below Mach 8, combustion in a scramjet engine can generate a large local pressure rise and separation of the boundary layer on the surfaces of the combustion duct. This separation, which can feed upstream of the point of fuel injection, acts to further diffuse the core flow in the duct, and will interact with the inlet, possibly causing an unstart of the engine. A short length of duct, called the isolator, is usually added to the scramjet flowpath upstream of the combustor to contain this phenomenon. In some engines the combination of the diffusion in the isolator and heat release in the combustor decelerate the core flow to subsonic conditions, in what is called dual-mode combustion. At speeds above Mach 8 the increased kinetic energy of the airflow through the engine means that the combustion generated pressure rise is not strong enough to cause boundary layer separation. Flow remains attached and supersonic throughout, and this is termed a pure scramjet. The quasi-one-dimensional analysis of pure scramjet flows is presented first, followed by analysis with the added complexity needed to deal with separated or dual-mode combustion flows.

A differential element of attached flow in a duct is shown in Fig.31. In this element, fuel and air are burning, and a friction force $dFr = \tau_w A_w$ is applied by the walls, together with a heat loss in the amount dQ. For simplicity of analysis, the flow is assumed to be that of a calorically perfect gas with ratio of specific heats, γ, gas constant R, and constant pressure specific heat, c_p. Combustion heat release is modeled through the use of a heat of combustion, h_{pr}, and the change in total enthalpy of the element is:

$$dH_t = h_{pr} f_{st} d\phi - dQ \qquad (7)$$

where f_{st} = stoichiometric fraction of fuel to air, and $d\phi$ = equivalence ratio of fuel that combusts in length dx.
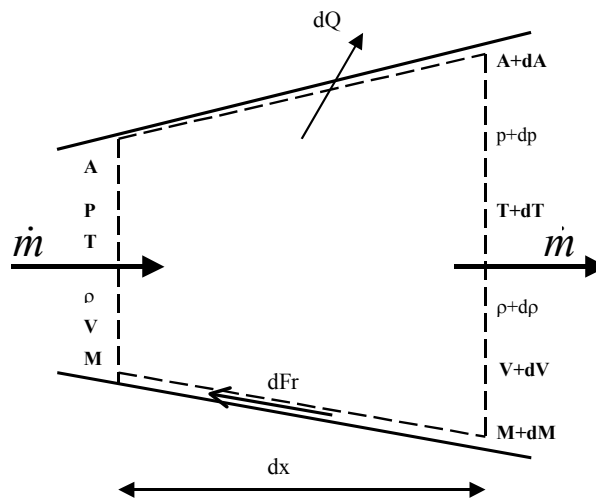

Figure 31 – differential element of combusting flow in a duct

The corresponding change in the total temperature of the flow is therefore $dT_t = dH_t/c_p$. The wall shear stress is related to a skin friction coefficient through $\tau_w = C_f \rho V^2/2$, and from the definition of the hydraulic diameter (D) of the duct, $A_w = 4Adx/D$. The differential conservation equations of mass, momentum and energy for the element, are therefore given by:

$$\frac{d\rho}{\rho} + \frac{dV}{V} + \frac{dA}{A} = 0 \qquad (8)$$

$$\frac{dp}{p} + \frac{\gamma M^2}{2}\frac{4C_f dx}{D} + \frac{\gamma M^2}{2}\frac{dV^2}{V^2} = 0 \qquad (9)$$

$$\frac{dT}{T} + \frac{\gamma-1}{2}M^2\frac{dV^2}{V^2} = \left(1 + \frac{\gamma-1}{2}M^2\right)\frac{dT_t}{T_t} \qquad (10)$$

Together with the equation of state for the gas and the definition of Mach number (in differential form):

$$\frac{dp}{p} - \frac{d\rho}{\rho} - \frac{dT}{T} = 0 \qquad (11)$$

$$\frac{dM^2}{M^2} - \frac{dV^2}{V^2} + \frac{dT}{T} = 0 \qquad (12)$$

we have five equations to relate the seven variables. Following Shapiro (1953), area change (dA/A) and total temperature change (dT_t/T_t) are treated as independent variables, and differential relations for all the others can be determined by elimination. The relation for Mach number is:

$$\frac{dM^2}{M^2} = \frac{2\left(1+\frac{\gamma-1}{2}M^2\right)}{1-M^2}\frac{dA}{A} + \frac{\left(1+\gamma M^2\right)\left(1+\frac{\gamma-1}{2}M^2\right)}{1-M^2}\frac{dT_t}{T_t} + \frac{\gamma M^2\left(1+\frac{\gamma-1}{2}M^2\right)}{1-M^2}4C_f\frac{dx}{D} \quad (13)$$

This relation may be integrated to determine the axial distribution of Mach number in ducts with specified area and total temperature distributions, along with a knowledge of C_f, and all the other 1-D flow properties of interest.

An example of the use of this methodology is plotted in Fig. 32, which shows the properties in a round combustor duct with an initial diameter of 0.06m and a divergence with area ratio of 2. In this instance the properties at the throat ($x_2 = 0.0$ m) are defined ($M_2 = 3.60$, $p_2 = 50$ kPa, $T_2 = 650$ K, $H_{t2} = 2.35$ MJ/kg) and hydrogen fuel ($h_{pr} = 119,954$ kJ/kg) is injected at $x_3 = 0.2$ m with an equivalence ration of $\phi = 0.50$. The amount of fuel that is allowed to react with the air at a particular station is dictated by a mixing efficiency curve, $\eta_m(X)$, that takes the form:

$$\eta_m = \eta_{m,e}\frac{\vartheta X}{1-X} \qquad (14)$$

where $\eta_{m,e}$ is the mixing at the end of the combustor, $X = (x-x_3)/(x_4-x_3)$ and ϑ is an empirical constant of order 1 to 10 which depends of the rate of mixing (Heiser & Pratt 1994).

M$_2$ = 3.60, p$_2$ = 50 kPa, T$_2$ = 650 K, H$_{t2}$ = 2.35 MJ/kg, φ = 0.50
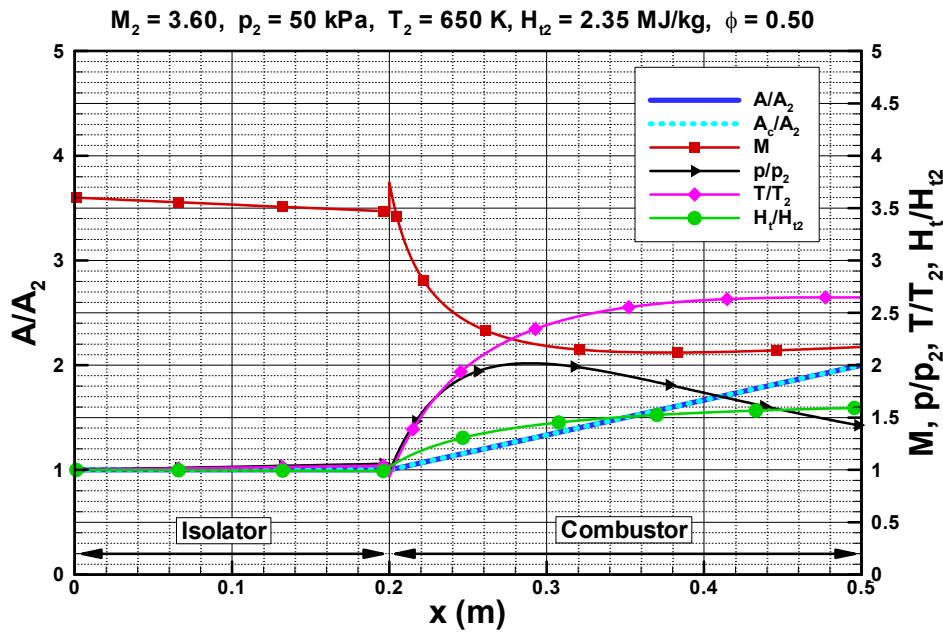

Figure 32 - Attached flow through an isolator and divergent combustor

For the current example, $\eta_{m,e}$ was set to 0.8 and a value of $\vartheta = 5.0$ was used. The heat release curve was therefore:

$$H_t = H_{t2} + h_{pr} f \phi \eta_m - dQ \qquad (15)$$

Skin friction was calculated based on a $C_f = 0.002$ and heat loss to the structure (dQ) was calculated using Reynolds analogy.

Given the limitation of constant ratio of specific heats (γ) and gas constant (R) in the analysis, eqn. 13 is integrated in sections along the duct. In the isolator section upstream of fuel injection, values of γ = 1.37 and R = 287 J/kgK were used. In the combustor, the properties of the real fuel/air/combustion products mixture varies with length, but average values of γ = 1.31 and R = 297 J/kgK were used. In the isolator section of the duct the Mach number reduces and the pressure and temperature increase due to the action of friction on the duct surfaces. At the start of the combustor, flow properties are recalculated to be consistent with the values of γ and R used in the combustor integration, while conserving fluxes of mass, momentum and total enthalpy across the boundary between the isolator and combustor. Fuel is also added, and combustion along the duct leads to a drop in the Mach number, an increase in the temperature, and the pressure varies smoothly in response to the competing effects of combustion and area increase. The peak pressure and temperature in the duct are $p/p_2 = 2.02$ and $T/T_2 = 2.65$. The analysis results in an estimate of the one-dimensional properties of the flow as it exits the combustor at $x_4 = 0.5$ m.

For the situation where flow separation occurs in the combustion region, the preceding analysis does not provide a useful model of the real flow, as the area of the core flow, A_c, is less than the geometric area. The core flow area represents a new variable, hence an extra relation is needed to close the problem. Figure 33 shows a sketch of a supersonic duct flow that has been separated by either combustion or some other imposed back-pressure (Ortwerth 2001). The core flow (region I) experiences a pressure gradient in the form of an area constriction and shock train in the supersonic region, and an area increase once it is decelerated to subsonic conditions. The separated flow (region III) balances the pressure gradient by shear

stress on its boundary with region II. The pressure gradient in the core flow must be equal to the pressure gradient that the shear can support in the separated region. Based on a large amount of experimental data at different Mach numbers, Reynolds numbers and duct geometries, the pressure ratio p/p_i over a length dx was determined by Ortwerth (2001) to vary as:

$$\frac{d(p/p_i)}{dx} = 4K\gamma(p/p_i)M^2 \qquad (16)$$

where $4K = 44.5C_{f0}$ and C_{f0} = the friction coefficient at the initial separation point.
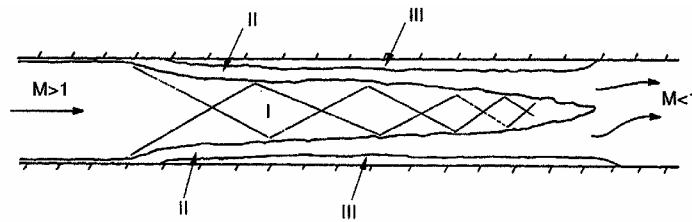

Figure 33 - Flow model for separation in a duct

This relationship essentially supplies a length scale required to achieve the full pressure rise.

A differential element of the separated flow in a duct is shown in Fig. 34. The main difference between this and Fig. 31 is that the core area (A_c) is less than the geometric area (A). The conservation equations all relate to the core area, but friction and heat loss are based on the geometric area. In this instance, the energy equation, equation of state and definition of Mach number are the same as for the attached flow, but the mass conservation and momentum equations are now:

$$\frac{d\rho}{\rho} + \frac{dV}{V} + \frac{dA_c}{A_c} = 0 \qquad (17)$$

$$\frac{dp}{p} + \frac{\gamma M^2}{2}\frac{4C_f dx}{D} + \frac{\gamma M^2}{2}\frac{A_c}{A}\frac{dV^2}{V^2} = 0 \qquad (18)$$
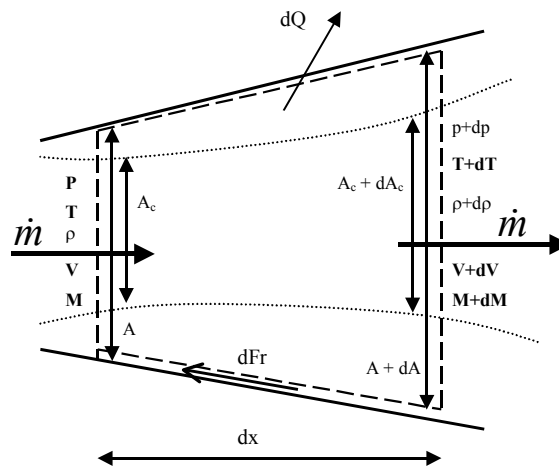

Figure 34 – Differential element of separated flow

Equation 16 is the extra relation required to close the separated flow problem. After a significant amount of algebraic manipulation, a relation for Mach number equivalent to eqn. 13 is as follows:

$$\frac{dM^2}{M^2} = -\left(1 + \frac{\gamma-1}{2}M^2\right)\left[\frac{dp/p}{\frac{\gamma M^2}{2}\frac{A_c}{A}} + \frac{4C_f\frac{dx}{D}}{\frac{A_c}{A}} + \frac{dT_t}{T_t}\right] \quad (19)$$

This must be integrated in conjunction with the following relation for A_c/A:

$$\frac{d(A_c/A)}{A_c/A} = \left[\frac{1-M^2\{1-\gamma(1-A_c/A)\}}{\gamma M^2 A_c/A}\right]\frac{dp}{p} + \left(\frac{1+(\gamma-1)M^2}{2A_c/A}\right)4C_f\frac{dx}{D} + \left(1+\frac{\gamma-1}{2}M^2\right)\frac{dT_t}{T_t} \quad (20)$$

An example of the use of this methodology is plotted in Fig. 35, which shows the properties in the same round combustor duct as Fig. 32, but with reduced throat Mach number and increased fuel equivalence ratio. In this instance the properties at the throat are $M_2 = 2.65$, $p_2 = 50$ kPa, $T_2 = 650$ K and $H_{t2} = 1.59$ MJ/kg. Hydrogen fuel is injected at $x_3 = 0.2$ m once again, and is assumed to combust with the same mixing curve as before (eqn. 14), but with an increased equivalence ratio of $\phi = 0.81$. The same values of γ and R were also used for the isolator and the combustor. At these conditions the pressure rise from combustion separates the duct boundary layer (Korkegi 1975). The position at which separation occurs is iteratively chosen such that the flow may re-attach smoothly in the divergent section. Furthermore, if the core flow reduces to subsonic conditions in the separated region (as in this case), the flow must re-attach subsonically and then re-accelerate through a thermal throat at an axial position that can be calculated apriori, as outlined in Shapiro (1953).
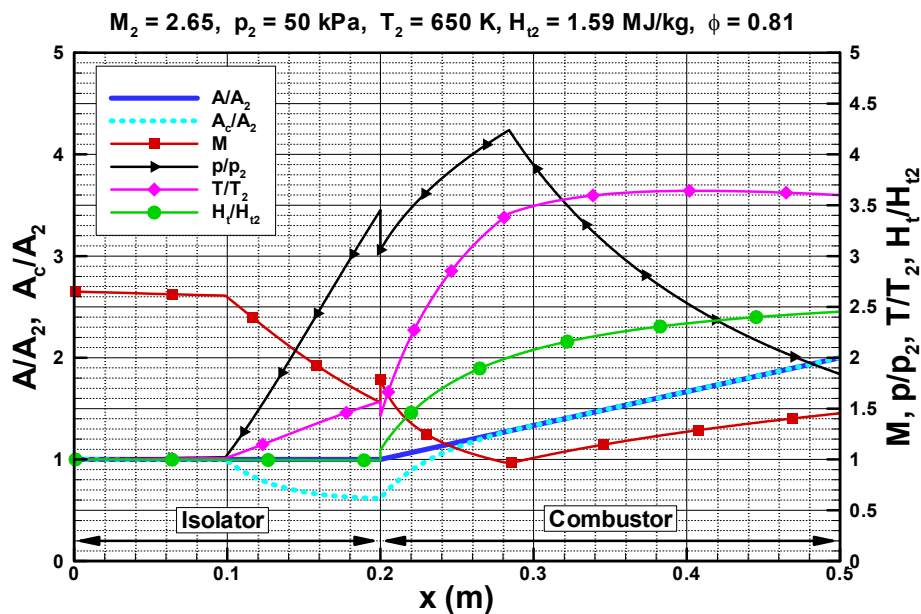

Figure 35 - Thermally throated, separated flow through a divergent duct

Figure 35 shows that the separation point that satisfies these criteria is at $x = 0.988$ m. The core flow begins diffusing at this point at a rate dictated by eqn. 16, reaching a minimum area of $A_c/A_2 = 0.616$. Combustion of fuel acts to push the flow towards re-attachment, which occurs at $x = 0.284$ m with M =

0.961. The flow then re-accelerates through the thermal throat at x = 0.295 m. Note that in comparison with the attached flow example (Fig. 32), the pressure and temperature rise in this dual-mode combustion flow are considerably higher, peaking at $p/p_2 = 4.24$ and $T/T_2 = 3.64$. While it is recognized that this analysis involves the significant assumption of a perfect gas, it does however contain all the physical attributes that are exhibited by real flows. Similar analyses of combustion flows in thermodynamic equilibrium are presented in Auslender & Smart (1999).

In the design of scramjet combustors there are some key issues that must be addressed in order to arrive at a useful configuration. These are:

1. Adequate mixing of fuel and air

2. Fuel ignition and flame holding

3. Operation over a range of inflow conditions

The perennial issue of fuel/air mixing can never be ignored in the design of a scramjet, and this issue becomes more difficult as the Flight Mach number increases. A multitude of fuel injection/mixing schemes have been examined by a multitude of researchers, including some interesting studies presented in Stalker et. al. (2006) and Northam et. al. (1991). Fuel ignition and flame holding are of course related to fuel mixing. Fuel injection schemes must not only generate fuel/air mixing, but enable ignition of fuel, followed by stablization of a combustion flame. At lower flight Mach numbers ignition aids such as spark plugs and highly reactive fuel additives are used to overcome ignition problems, although fuel addatives can affect the specific impulse of the engine if these are required on a continuous basis. In many instances it is desirable to operate a scramjet over a range of flight conditions, resulting in flow entering the combustor at a range of inflow conditions. Fuel scheduling from multiple injection sites is often used to increase the operational range of a scramjet combustor.

4.1.3   Expansion

The expansion process converts the potential energy of the combusting flow to kinetic energy and then thrust. In an airframe-integrated scramjet, this begins in the divergent sections of the combustor and internal nozzle, and continues over a large portion of the vehicle afterbody. The shape of the afterbody also determines the direction of the gross thrust vector relative to the vehicles flight direction. An ideal expansion nozzle would expand the engine plume isentropically to the freestream pressure assuming chemical equilibrium, and this is the usual criterion that real nozzle flows are measured against. Loss mechanisms in practical expansion processes are due to:

1. Under-expansion

2. Failure to recombine dissociated species

3. Flow angularity

4. Viscous losses

The weight of a fully-expanding internal nozzle/aftbody would be prohibitive at most hypersonic flight conditions, hence under-expansion losses are usually traded against vehicle structural weight. Dissociation losses result from chemical freezing in the rapid expansion process in the nozzle, essentially locking up energy that cannot be converted to thrust. This problem can be exacerbated by inefficient compression, which leads to higher than necessary temperatures at the start of the expansion process. Flow angularity losses are a product of varying flow directions in the nozzle, and viscous losses are associated with friction on the internal nozzle and afterbody surfaces.

The aforementioned expansion losses are typically modelled using a nozzle efficiency parameter, η_N, which is applied as a gross thrust coefficient to the ideal stream thrust increment between the end of the

combustor (station 4) and the end of the vehicle (station 10). The ideal stream thrust increment is calculated by isentropically expanding the flow at station 4 assuming chemical equilibrium to either, (1) a specified area based on an estimate of the size of the expanded plume, or (2) a specified pressure greater than or equal to the freestream pressure. Typical values for the nozzle efficiency range between $\eta_N = 0.85\text{-}0.95$. At the completion of this analysis, an estimate of the 1-D properties at the vehicle exit is obtained, and the based on eqn. 3, an estimate of the uninstalled thrust of a scramjet can be calculated.

It would be fair to say that the design of nozzle expansion systems for airframe-integrated scramjet vehicles is one of the least mature aspects of overall design process. This may be due to the historical separation of the propulsion and airframe, with neither groups wanting to take full responsibility for the engine nozzle/vehicle afterbody. This difficulty is exacerbated by the fact that the character of the engine plume can vary greatly with flight Mach number and engine throttle level. The engine plume can also affect the performance of vehicle trim surfaces and flaps. Despite this, confidence that these issues can be solved for practical vehicles was significantly increased by the successful flights of the NASA's Hyper-X vehicle.

5.0   SCRAMJET APPLICATIONS

The "holy grail" of hypersonic airbreathing propulsion is its use as part of a system for reaching low earth orbit, either for satellites insertion or manned operations. At the current stage of scramjet technology development, single-stage-to-orbit systems are not viable, however many multi-stage options have been studied (Meht & Bowles 2001, Bowcutt et. al. 2002). Turbojets are a propulsion candidate for the initial phase of a flight to LEO, but are currently limited to Mach 3+. Scramjets are a desirable candidate for the middle phase, particularly if the upper limit of their operation can be stretched to Mach 10+. However, scramjet use in conjunction with turbojets is problematic, as the take-over Mach number of a scramjet designed to operate at Mach 10 and above is likely to be Mach 5-6, in the absence of significant variable geometry. An efficient liquid fuelled rocket is a desirable candidate for the last phase to LEO.

An example of a possible system for acceleration to low earth orbit is described here, based on a rocket-scramjet-rocket three-stage vehicle design to lift approximately 100 kg to LEO. The first stage is a solid rocket, chosen for its simplicity of operation, despite its low efficiency. The second stage is a scramjet powered hypersonic vehicle with an initial mass of 3000 kg that can operate between Mach 6 and 12. This is followed by a liquid fuelled rocket third stage to boost the payload to LEO.

5.1   Vehicle Description

Booster

The initial booster is required to achieve flight conditions suitable for operation of the scramjet from a ground launch. A preliminary sizing of this booster was made assuming solid fuel rocket motors, structural mass fraction $m_s/m_o = 0.18$, Isp of 270 seconds at sea level and 276 seconds in vacuum and aerodynamic data from a typical ballistic launch vehicle such as Ariane 3 (Isakowitz 1995). The requirements of the booster were that it place the 3000 kg scramjet powered second stage at an altitude of 27 km, travelling at Mach 6 with a flight path angle of $\zeta = 0.0^{\circ}$. An initial mass of $m_o = 10300$ kg was estimated from this preliminary analysis assuming an easterly, equatorial launch. Optimisation of the boost trajectory or use of a higher performing rocket would lead to a reduced m_o.

Scramjet Powered Hypersonic Vehicle

Waveriders are a class of hypersonic vehicles that have the capacity for high lift-to-drag ratio (L/D). These vehicles accomplish this by "riding" the shock wave they produce during flight, which theoretically remains attached to the sharp leading edges of the vehicle. These vehicles were taken beyond academic

interest by researchers at the University of Maryland who optimised their shape to maximise $L/D(Volume)^{2/3}/A_{planform}$, and accounted for viscous effects (Bowcutt et. al. 1987). Integration of scramjet propulsion systems into waverider-derived hypersonic vehicles has also been studied (O'Neill & Lewis 1992). The current concept involves the use of a scramjet-powered vehicle based on a waverider developed for Mach 14 flight (Gillum & Lewis 1997). From the predetermined start mass of 3000kg and the average density for a hydrogen fuelled hypersonic vehicle, including payload, of $124 kg/m^3$ (Lewis 2001), the volume of the vehicle was 24.19 m³. Scaling up the waverider model to match this volume results in a vehicle with length = 12.59 m, span = 5.23 m and A$_{planform}$ = 39.05 m².

The experimentally determined aerodynamic coefficients of this waverider are listed in Norris (2006) for flight Mach numbers 6, 8, 10 and 14, indicating that the minimum vehicle drag occurs at $\alpha = -5^o$. These coefficients were used in this study for the scramjet-powered phase of the trajectory. In the force accounting methodology used here, the forebody drag of the vehicle was accounted to the propulsion system, whereas the external drag of the propulsion system was accounted to the vehicle. Furthermore, installation of the scramjet modules was assumed to have little effect on the overall vehicle lift.

The scramjet propulsion system used in the study was based on the Rectangular-to-Elliptical Shape Transition (REST) Scramjet configuration (Smart 1999, Smart 2001). This is a three-dimensional, fixed geometry, scramjet flowpath that is integrated with the vehicle forebody, transitions from a rectangular capture area to an elliptical throat, and includes an elliptical combustor. The particular configuration used here was developed for flight between Mach 6 and 12 with hydrogen fuel. Two views of how multiple RESTM12 modules would appear installed on a waverider are shown as Figs. 36(a) and (b).
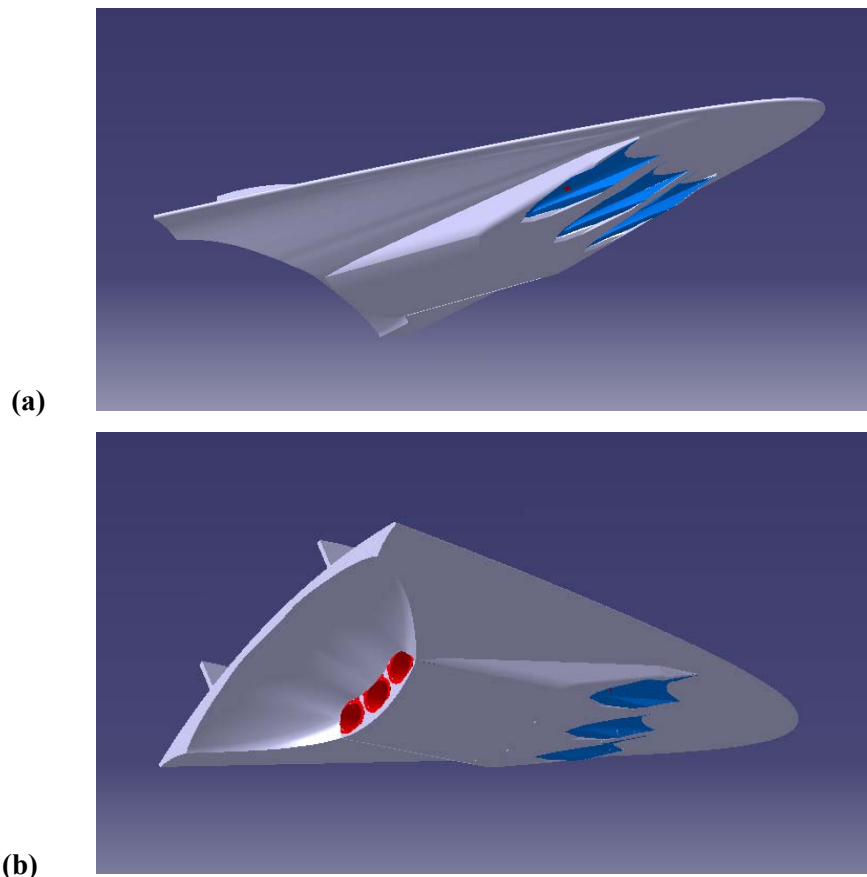
(a)

(b)

Figure 36 - Hypersonic waverider with RESTM12 scramjet propulsion system installed

Orbital stage

The orbital stage was a separate rocket that would be deployed from the scramjet vehicle payload bay and accelerate the payload from scramjet shut-down conditions to the required 200km circular orbit. A structural mass fraction of 0.15 was used for the orbital stage with Isp = 324s. These values were taken from the upper stage of the Japanese H2 launch vehicle (Isakowitz 1995). From the mass, velocity, altitude and flight path angle at scramjet shutdown, the payload mass was approximated using Hohmann transfers. The orbital stage provided the propulsion to insert the payload into a low earth transfer orbit with an apogee altitude of 200km and then to circularize the orbit at 200km.

5.2   Trajectory Simulation

The software used for trajectory simulation was a Fortran based code, originally developed at the Space Systems Institute in Stuttgart, Germany. The dynamic equations were taken from Burkhardt (2001) and describe a 3 degree-of-freedom trajectory over a rotating earth model, using a 4th order Runge-Kutta integration technique. A spheroidal earth model was used to determine the radius of the Earth at given latitudes. A 4th order gravitational model (Regan & Anandakrishnan 1993) was implemented to approximate the Earth's gravitational field, and the atmospheric parameters were calculated using the Mass Spectrometer Incoherent Scatter Experiment 1993 (MSISE 93) atmosphere model (Tetlow 2003).

The boost flight segment was controlled by a launch elevation, azimuth and position. The scramjet flight phase was controlled using a parameter set of angle-of-attack as a function of time. The aim of the control strategy was to achieve as high an altitude and flight path angle as possible at a shut-off flight Mach number close to 12. The trajectory was also controlled to maintain dynamic pressure between 50 and 100kPa. Although several runs were performed to understand the dominant parameters governing the trajectory, no optimisation of the scramjet phase was performed in this preliminary study.

5.3   Scramjet Propulsion Database Generation

The propulsion module used for the example follows the form outline in section 4, and it was developed from the calculated performance of a fixed geometry, REST scramjet engine that has a design point of M_0 = 12.0, but remains operational down to M_0 = 6.0. This engine will be referred to here as the RESTM12 scramjet and is considered to be a near-term configuration that could be envisaged to fly within the 5-10 years.

During a trajectory calculation the trajectory program makes calls to the propulsion module to obtain the specific thrust, specific impulse, and equivalence ratio of the engine for a particular flight velocity, angle-of-attack and altitude. The RESTM12 scramjet is designed to operate at $q_0 \sim 50$ kPa in conjunction with a vehicle forebody compression equivalent to that generated by a 6° wedge. Analysis of the waverider vehicle forebody over the Mach 6-12 flight regime indicated that at $\alpha = 0^o$ it generates a pre-compression equivalent to an 8° wedge. Given this, the nominal angle-of-attack for the vehicle was assumed to be $\alpha = -2^o$. Hence the engine was installed on the vehicle so that the thrust vector of the engine was parallel with the velocity vector when the vehicle was at $\alpha = -2^o$. The operational angle-of-attack range for the engine was assumed to be +/- 3 deg. about the nominal, so that the angle-of-attack limits for the vehicle were set to $\alpha = -5^o$ and $+1^o$. As already mentioned, the vehicle had minimum drag and zero lift at $\alpha \sim 5^o$.

A database was created for the RESTM12 flowpath using the compression, combustion and nozzle expansion models described in section 4. This was based on calculations performed for M_0 = 6.0, 8.0, 10.0 and 12.0, at vehicle $\alpha = -6.0, -4.0, -2.0, 0.0$ and $+2.0$ degrees, and $q_0 = 50$ kPa. All calculations were performed with $\phi = 1.0$, except for the $M_0 = 6.0$ calculations, where the engine reached its operability limit at $\phi < 1.0$. This characteristic was due to the fact that the RESTM12 scramjet was designed with a contraction ratio and combustor divergence suitable for operation at $M_0 > 10$, and is one of the real world compromises that must be made in a fixed geometry engine.

The three propulsion parameters required by the trajectory code were the uninstalled specific thrust, $f = \Delta F/\dot{m}_0 = (F_{10} - F_0)/\dot{m}_0$, the specific impulse of the engine, $\mathrm{Isp} = \Delta F/(g*\dot{m}_f)$, and equivalence ratio, $\phi = \dot{m}_f/(f_{st}*\dot{m}_0)$. The calculations used in the database were performed for a single engine with a capture width, $w_{cap} = 0.15$ m; i.e. at wind-tunnel model scale. It was assumed that the propulsion parameters calculated in this way can be conservatively used for larger engines. A lower limit of $q_0 = 30$ kPa was placed on the use of the database due to kinetic limitations related to low pressures entering the combustor. Three RESTM12 scramjet modules were used for the baseline trajectory calculation discussed in the next section, each with a width of $w_{cap} = 0.76$ m. This scale allowed smooth integration with the 12.59 m length vehicle.

5.4   Baseline LEO Trajectory

The solid rocket booster supplied the 3000 kg scramjet powered vehicle at an altitude h = 27 km, velocity V = 1804.5 m/s, and flight path angle of $\zeta = 0.0$ degrees. This corresponds to a flight Mach number M = 6.01 and dynamic pressure q = 48.0 kPa. An equatorial launch in an easterly direction was also assumed. Figure 37 shows M_0, q_0 and α for a baseline 272.5 second scramjet powered acceleration that reached $M_0 = 11.73$ at scramjet shutdown. The dynamic pressure was controlled through variation of angle-of-attack to stay within the required range (50-100 kPa). Note that α was kept between –4.0 and –5.0 degrees to accomplish this, indicating that the high lift capability of the vehicle was not utilized. A key result of this preliminary analysis appears to be that high L/D is not required for hydrogen fuelled scramjets.
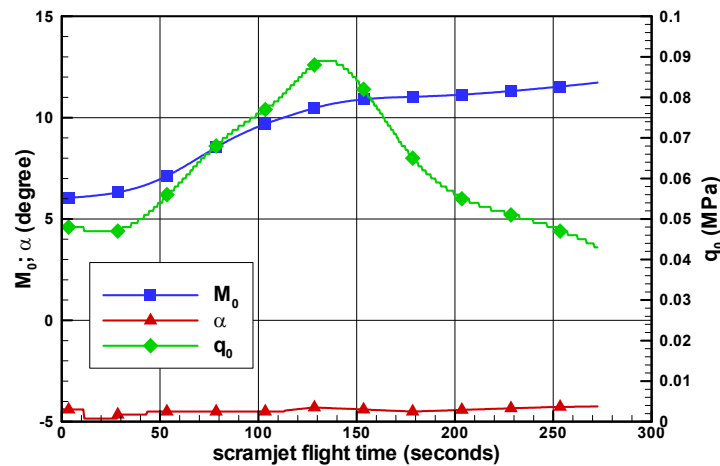

Figure 37 - Flight Mach number, angle-of-attack and dynamic pressure of baseline trajectory

Figure 38 shows plots of vehicle drag and engine thrust over the trajectory, along with the vehicle mass. Positive net thrust (Thrust-Drag) is key to achieving useful ΔV with the available fuel. Figure 38 indicates that up to $M_0 \sim 11$ the vehicle maintained a strong level of net thrust, whereas above $M_0 = 11$ net thrust was diminishing. Figure 39 shows plots of vehicle altitude and velocity during the scramjet powered phase, indicating an altitude of h = 37.15 km and velocity of V = 3745 m/s at scramjet shutdown. The scramjet consumed 1356 kg of hydrogen fuel (45.2% of the vehicle starting mass) and covered 807.6 km, leaving a vehicle mass at the end of the scramjet phase of 1644 kg.
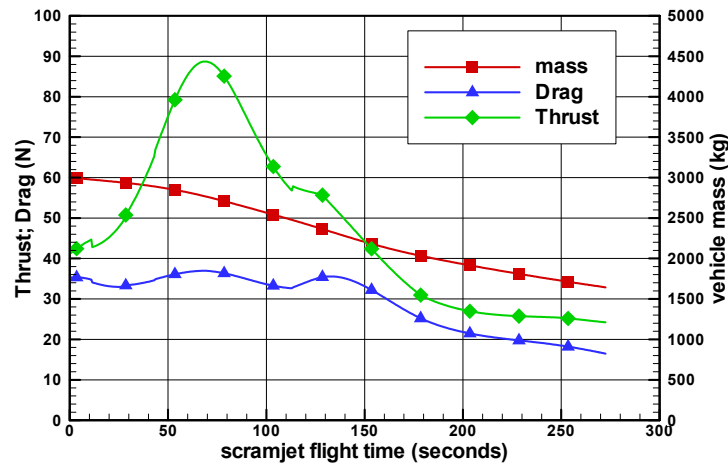
Figure 38 - Thrust, Drag and vehicle mass for the baseline trajectory
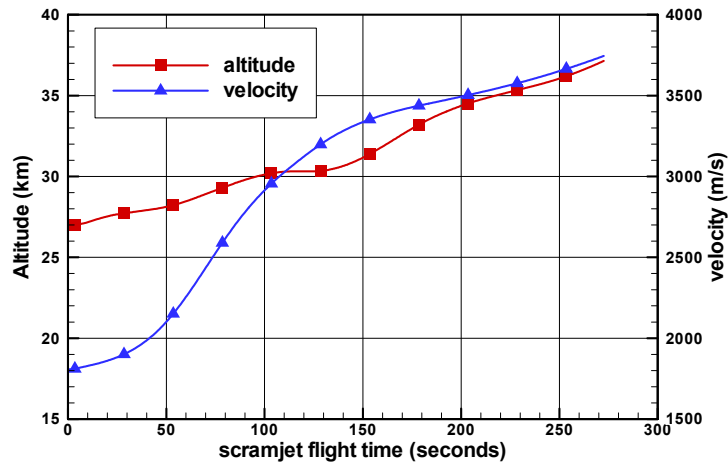

Figure 39 - Altitude and velocity of baseline trajectory

A fortunate aspect of the trajectory was that the vehicle was able to operate close to its minimum drag orientation for most of the scramjet powered flight. This was possible because of the low lift requirements of the vehicle. Furthermore, assuming a fuel density of 85 kg/m³ consistent with slush hydrogen, 1356 kg of fuel corresponds to a volume of 15.95 m³, which is 65.9% of the entire vehicle volume. It would appear that a waverider most suitable for access-to-space applications should be optimised for maximum $(Volume)^{2/3} / A_{planform} / C_D$. Trajectory optimisation for maximum fuel efficiency was not performed here, but would result in reduced fuel consumption.

Analysis of the Hohmann transfers required to lift the final stage to a 200 km circular orbit indicated a final payload mass of 102.7 kg. Recalling that the estimated launch mass of the system was 10300 kg, the current analysis results in a payload fraction $m_p/m_0 = 0.0997 \sim 1\%$. This preliminary result is promising enough to consider refinements to the analysis (including trajectory optimization of boost and scramjet phases) and a higher performing booster. Greatest improvement in the scramjet phase would result from increased net thrust at Mach 10+. This could be achieved through higher engine thrust and/or reduced vehicle drag.

REFERENCES

Anderson, G.Y., McClinton, C.R. and Weidner, J.P., 2001, "Scramjet Performance", Scramjet Propulsion, Progress in Astronautics and Aeronautics, AIAA Washington DC, Chapter 6.

Andrews, E.H., 2001, "Scramjet development and testing in the United States", AIAA paper 2001-1927.

Andrews, E. H., McClinton, C. R, and Pinckney, S. Z., 1971, "Flowfield Starting Characteristics of an Axisymmetric Mixed-Compression Inlet," NASA TM-X-20n.

Andrews, E.H. and Mackley, E.A., 1994, "Review of NASA's Hypersonic Research Engine Project", NASA TM 107759; also AIAA paper 93-2323.

Auslender, A.H., and Smart, M.K., 2000, "Comparison of Ramjet Isolator Performance with Emphasis on Non-Constant Area Processes", 2000 Joint Army-Navy-NASA-Air Force (JANNAF) Meeting, Monterey, California.

Barthelemy, R.R., 1989, "The National Aero-Space Plane Program", AIAA Paper 89-5001.

Billg, F.S., 1995, "Supersonic combustion ramjet missile", Journal of Propulsion and Power, 11(6), p1139-1146.

Bowcutt, K.G., Anderson, J.D., and Capriotti, D., 1987, "Viscous Optimized Hypersonic Waveriders", AIAA paper 87-0272.

Bowcutt, K., Gonda, M., Hollowell, S. and Ralston, S., 2002, "Performance, operational and economical drivers of reusable launch vehicles", AIAA paper 2002-3901.

Burkhardt, J., 2000, "REENT6D a Simulation and Optimization Tool for Re-entry Missions" IRS - Internal report IRS-01B7: Stuttgart.

Curran, E.T., 2001, "Scramjet engines: The first forty years", Journal of Propulsion and Power", 17(6), p1138-1148.

Cain, T., Owens, R. and Walton, C., 2004, "Reconstruction of the HyShot 2 Flight from Onboard Sensors" Fifth Symposium on Aerothermodynamics for Space Vehicles, Cologne, Germany.

Ferlemann, S.M., McClinton, C.R., Rock, K.E. and Voland, R.T., 2005, "Hyper-X Mach 7 scramjet design, ground test and flight results", AIAA paper 2005-3322.

Ferri, A., 1964, "Review of the problems in application of supersonic combustion", Journal of the Aeronautical Society, 64(645), p575-597.

Gillum, M.J., and Lewis, M.J., 1997, "Experimental Results on a Mach 14 Waverider with Blunt Leading Edges", Journal of Aircraft, 34(3), pp 296-303.

Goldberg, T. J., and Hefner, J. N., 1971, "Starting Phenomena for Hypersonic Inlets with Thick Boundary Layers at Mach 6," NASA TN-D6280.

Gurylev, V. G., and Mamet'yev, Yu. A., 1978, "Effect of Cooling of the Central Body on Start-Up Separation of the Flow at the Intake and the Throttling Characteristics of Air Scoops at Supersonic and Hypervelocity Velocities," *Fluid Mechanics-Soviet Research,* Vol. 7, No. 3.

Heiser, W.H. and Pratt, D.T., 1994, "Hypersonic Airbreathing Propulsion", AIAA Education Series.

Henry, J.R. and Anderson, G.Y., 1973, "Design considerations for the airframe-integrated scramjet", NASA TM X-2895.

Huebner, L.D., Rock, K.E., Ruf, E.G., Witte, D.W. and Andrews, E.H., 2001, "Hyper-X flight engine ground testing for flight risk reduction", Journal of Spacecraft and Rockets, 38(6), p844-852.

Hunt, J.L. and Rausch, V.L., 1998, "Airbreathing hypersonic systems focus at NASA Langley Research Center", AIAA paper 98-1641.

Isakowitz, S.J., 1995, "International Reference Guide to Space Launch Systems", AIAA.

Kantrowitz, A., and Donaldson, C., 1945, "Preliminary Investigation of Supersonic Diffusers," NACA WRL-713.

Korkegi, R.H., 1975, "Comparison of shock induced two- and three-dimensional incipient turbulent separation", AIAA Journal 13(4), p534-535.

Lewis, M.J., 2001, "Significance of Fuel Selection for Hypersonic Vehicle Range", Journal of Propulsion and Power, 17(6).

Mahoney, J. J., 1990, *Inlets for Supersonic Missiles,* AIAA Education Series, AIAA Washington, DC.

McClinton, C.R., 2006, "X-43 – scramjet power breaks the hypersonic barrier: Dryden lectureship in research for 2006", AIAA paper 2006-1.

Mehta, U.B., and Bowles, J.V., 2001, "A two-stage-to-orbit spaceplane concept with growth potential", Journal of Propulsion and Power, 17(6).

Norris, J.D., 2006, "Mach 8 High Reynolds Number Static Stability Capability Extension Using a Hypersonic Waverider at AEDC Tunnel 9", AIAA paper 2006-2815.

Northam, G.B., Capriotti, D.P., Byington, C.S. and Greenberg, I., 1991, "Mach 2 and Mach 3 mixing and combustion in scramjets", AIAA paper 91-2394.

O'Neill, M.K., and Lewis, M.J., 1992, "Optimized Scramjet Integration on a Waverider", Journal of Aircraft, 29(6), pp1114-1121.

Ortwerth, P.J., 2001, "Scramjet Vehicle Integration", Scramjet Propulsion, Progress in Astronautics and Aeronautics, AIAA Washington DC, Chapter 17.

Pandolfini, P.P., 1986, "Instructions for using ramjet performance analysis (RJPA) IBM-PC Version 1.0", JHU-APL NASP-86-2.

Paull, A., Alesi, H. and Anderson, S.,2002, "HyShot Flight Program and how it was developed", AIAA 02-4939.

Pinckney, S.Z., Ferlemann, S.M.,Mills, J.C. and Bass, L.S., 1994, "Program manual for SRGULL version 2.0", HX#829.1.

Rausch, V.L., McClinton, C.R. and Crawford, J.L., 1997, "Hyper-X: flight validation of hypersonic airbreathin technology", AIAA paper 97-7024.

Regan, F.J., and Anandakrishnan, S.M., 1993, "Dynamics of Atmospheric Reentry," AIAA Education Edition.

Schweikart, L., 1998, "The Hypersonic Revolution – Case Studies in the History of Hypersonic Technology – Volume III", Air Force History and Museums Program, Bolling AFB, DC, 20332-1111.

Shapiro, A.H., 1953, "The dynamics and thermodynamics of compressible fluid flow", John Wiley & Sons, New York.

Smart, M.K., 1999, "Design of Three-Dimensional Hypersonic Inlets with Rectangular-to-Elliptical Shape Transition", Journal of Propulsion and Power, Vol. 15, No. 3, pp 408-416.

Smart, M.K., 2001, "Experimental Testing of a Hypersonic Inlet with Rectangular-to-Elliptical Shape Transition", Journal of Propulsion and Power, Vol. 17, No. 2, pp 276-283.

Smart, M.K., Hass, N.E. and Paull, A., 2006, "Flight Data Analysis of the HyShot 2 Flight Experiment", AIAA Journal, Vol. 44, No. 10, pp 2366-2375.

Smart , M.K. and Tetlow, M. R., 2006, "Orbital delivery of small payloads using hypersonic airbreathing propulsion", AIAA paper 2006-8019.

Stalker, R.J., Paull, A., Mee, D.J., Morgan, R.G. and Jacobs, P.A., 2006, "Scramjets and shock tunnels – the Queensland experience", Progress in Aerospace Sciences, 41, p471-513.

Tetlow, M., 2003, "Commercial Launch Vehicle Design and Predictive Guidance Development," Ph. D. Dissertation, School of Mechanical Engineering, The University of Adelaide.

Trexler, C.A. and Souders, S. W., 1975, "Design and performance at a Mach number of 6 of an inlet for an integrated scramjet concept", NASA TN D-7944.

Van Wie, D. M., 2001, "Scramjet Inlets", Scramjet Propulsion, Progress in Astronautics and Aeronautics, AIAA Washington DC, Chapter 7.

Voland, R. and Rock, K.E., 1995, "NASP concept demonstration engine and sub-scale parametric engine tests", AIAA paper 95-6055.

Voland, R.T., Rock, K.E., Huebner, L.D., Witte, D.W., Fischer, K.E. and McClinton, C.R., 1998, "Hyper-X engine design and ground test program", AIAA paper 98-1532.

Voland, R.T., Auslender, A.H. Smart, M.K. Roudakov, V.L., Semenov, V.L. and Kopchenov, V., 1999, "CIAM/NASA Mach 6.5 Scramjet Flight and Ground Test", AIAA paper 99-4848.

Waltrup. P.J., Billg, F.S. and Stockbridge, R.D., 1982, "Engine sizing and integration requirements for hypersonic airbreathing missile applications", AGARD-CP-207, No. 8.

Waltrup, P.J., 1987, "Hypersonic airbreathing propulsion: evolution and opportunities", AGARD CP-428, No. 12.

Waltrup, P.J., 1990, "The dual combustor ramjet: a versatile propulsion system for hypersonic tactical missile applications", AGARD CP-527, No. 7.

Webber, R.J. and MacKay, J.S., 1958, "An analysis of ramjet engines using supersonic combustion", NACA TN 4386.